Ho-Hagemann, H.T.M.; Groeger, M.; Rockel, B.; Zahn, M.; Geyer, B.;
Meier, H.E.M.:

Effects of air-sea coupling over the North Sea and the Baltic Sea on simulated summer precipitation over Central Europe

In: Climate Dynamics (2017) Springer

DOI: 10.1007/s00382-017-3546-8

Effects of air-sea coupling over the North Sea and the Baltic Sea on simulated summer precipitation over Central Europe

Ha Thi Minh Ho-Hagemann[1], Matthias Gröger[2], Burkhardt Rockel[1], Matthias Zahn[1], Beate Geyer[1], H.E. Markus Meier[3,2]

[1]Institute for Coastal Research, Helmholtz Zentrum Geesthacht, Germany (Ha.Hagemann@hzg.de)

[2]Swedish Meteorological and Hydrological Institute – SMHI, Sweden

[3]Leibniz Institute for Baltic Sea Research Warnemünde, Germany

Abstract

This study introduces a new approach to investigate the potential effects of air-sea coupling on simulated precipitation inland over Central Europe. We present an inter-comparison of two regional climate models (RCMs), namely, the COSMO-CLM (hereafter CCLM) and RCA4 models, which are configured for the EURO-CORDEX domain in the coupled and atmosphere-only modes. Two versions of the CCLM model, namely, 4.8 and 5.0, join the inter-comparison being almost two different models while providing pronouncedly different summer precipitation simulations because of many changes in the dynamics and physics of CCLM in version 5.0. The coupling effect on the prominent summer dry bias over Central Europe is analysed using seasonal (JJA) mean statistics for the 30-year period from 1979 to 2009, with a focus on extreme precipitation under specific weather regimes. The weather regimes are compared between the coupled and uncoupled simulations to better understand the mechanism of the coupling effects.

The comparisons of the coupled systems with the atmosphere-only models show that coupling clearly reduces the dry bias over Central Europe for CCLM 4.8, which has a large dry summer bias, but not for CCLM 5.0 and RCA4, which have smaller dry biases. This result implies that if the atmosphere-only model already yields reasonable summer precipitation over Central Europe, not much room for improvement exists that can be caused by the air-sea coupling over the North Sea and the Baltic Sea. However, if the atmosphere-only model shows a pronounced summer dry bias because of a lack of moisture transport from the seas into the region, the considered coupling may create an improved simulation of summer precipitation over Central Europe, such as for CCLM 4.8. For the latter, the benefit of coupling varies over the considered timescales. The precipitation simulations that are generated by the coupled system COSTRICE 4.8 and the atmosphere-only CCLM 4.8 are mostly identical for the summer mean. However, the COSTRICE simulations are generally more accurate than the atmosphere-only CCLM simulations if extreme precipitation is considered, particularly under Northerly Circulation conditions, in which the airflow from the North Atlantic Ocean passes the North Sea in the coupling domain. The air-sea feedback (e.g., wind, evaporation and sea surface temperature) and land-sea interactions are better reproduced with the COSTRICE model system than the atmosphere-only CCLM and lead to an improved simulation of large-scale moisture convergence from the sea to land and, consequently, increased heavy precipitation over Central Europe.

Keywords: regional climate model, Central Europe, EURO-CORDEX, dry bias, extreme precipitation, air-sea coupling

1 Introduction

Air-sea interactions and feedback are very important processes to bridge two main components of climate systems, namely, the atmosphere and ocean, but these components have often been neglected in previous stand-alone regional atmospheric or ocean models. Stand-alone atmospheric models that use prescribed sea-surface temperatures have been widely used for climate simulations and projections at the regional scale. However, fine-scale feedbacks that are associated with air-sea interactions can substantially influence the spatial and temporal structure of regional climates. A typical example is the Indian Ocean and its effects on the South Asia monsoon, for which air-sea feedbacks are essential in regulating the development of the South Asia monsoon (e.g., Meehl 1994). Ratnam et al. (2009) coupled the regional atmospheric model RegCM3 with the regional ocean model ROMS over the Indian Ocean and found that the coupling considerably improved the simulation of the Indian monsoon rain band over both the ocean and land areas. The Max-Planck ocean model MPI-OM, which was coupled to the regional climate model REMO, was employed over the Indonesian region and showed a remarkable improvement in the simulation of rainfall (Aldrian et al. 2005). Some studies noted that air-sea coupling could affect regional climate simulations in both the present climate (Artale et al. 2009; Nabat et al. 2015) and future scenarios (Somot et al. 2008).

Several regional coupled atmosphere-ocean system models (AORCMs) have been developed during the past two decades for northern European regions (e.g., Gustafsson et al. 1998; Hagedorn et al. 2000; Rummukainen et al. 2001; Döscher et al. 2002; Schrum et al. 2003; Dieterich et al. 2013; Tian et al. 2013; Ho-Hagemann et al. 2013, 2015; Pham et al. 2014; Wang et al. 2015; Gröger et al. 2015, Schrum 2016). The first regional coupled atmosphere - sea ice - ocean models were developed to improve short-range weather forecasts (e.g., Gustafsson et al. 1998) and study the processes and effects of coupling on the air-sea exchange (e.g., Hagedorn et al. 2000; Schrum et al. 2003). Over the past decade, the use of coupled models was extended to studies on climate change, particularly for the Baltic Sea (e.g., Rummukainen et al. 2001; Räisänen et al. 2004; Meier et al. 2011). Only a few current AORCMs cover the North Sea, so the potential effects of air-sea coupling over this area are still missing in the literature. In this study, we analyse two AORCMs in which the ocean models cover both the Baltic Sea and North Sea to to provide this missing information.

The effect of air-sea coupling on simulated temperature and precipitation appears not only over the ocean coupling domain but also inland (e.g., Somot et al. 2008; Ratnam et al. 2009; Pham et al. 2014; Ho-Hagemann et al. 2015). Li (2006) indicated that varying the SST over the Mediterranean Sea could initiate atmospheric teleconnections, which can influence precipitation in remote regions such as the Europe-Atlantic region. These changes in precipitation are associated with high-pressure anomalies and low-level wind convergence over the Europe-Atlantic region and air mass transport from the ocean (see Fig. 4, Li 2006). Ho-Hagemann et al. (2015) noted that both large-scale moisture convergence from the Mediterranean Sea and moisture sources from the North Atlantic Ocean that pass the North Sea contributed to the generation of heavy rainfall over Central Europe during phase 2 of the Oder flood event in July 1997. Excessively small large-scale moisture convergence from the oceans to the continental area led to the large dry bias of the atmosphere-only CCLM over Central Europe during this extreme event. The large-scale moisture convergence was improved in the air-sea coupled system model, and the dry bias was strongly reduced (Ho-Hagemann et al. 2015).

A precipitation dry bias over large areas of mid-latitude continents is a common problem for many atmospheric models (Vidale et al. 2003). Several studies in Central and Eastern Europe noted a dry bias in many regional climate models (RCMs) during the summer, such as in the assessment for the MERCURE project (Hagemann et al. 2001, 2004) and the joint standard evaluation for the EURO-CORDEX RCM ensemble (Kotlarski et al. 2014). This so-called summer drying problem is a long-standing problem that is still neither fully understood nor resolved for many RCMs. This dry bias should be reduced as much as possible before the respective climate models are applied to perform climate

projections so that more precise climate scenarios can be obtained. For example, a potential consequence of the summer drying problem is an incorrect analysis of changes in extreme precipitation based on climate projections and hindcast simulations. Here, the extreme precipitation is underestimated in both hindcasts and projections, but the projection bias, and thus the climate change signal, is highly uncertain because the bias behaviour is nonlinear due to changes in land-atmosphere coupling with future global warming. In this respect, Seneviratne et al. (2006) stated that a new transitional climate zone between dry and wet climates with strong land–atmosphere coupling would form in Central and Eastern Europe due to the northward shift of climatic regimes in Europe in response to increasing anthropogenic GHG concentrations. Thus, a low bias of precipitation in today's wet climate may not cause a relevant positive soil moisture precipitation feedback. The same bias in this future transitional climate can initiate such a positive feedback loop, thereby enhancing the low bias and hence causing an overly strong drying signal in precipitation.

The summer drying problem may have various origins that differ across models because of the complexity of the processes that may affect precipitation over Central Europe (Hagemann et al. 2004). Many different physical processes may contribute to this problem, including large-scale biases such as subsidence (RAACS Project; Machenhauer et al. 1998) or physical parameterisations such as radiation and land surface processes (see Betts et al. 1996; Seneviratne et al. 2002; Hagemann et al. 2001, 2004). Hagemann et al. (2004) investigated five RCMs and found that systematic errors in the atmospheric dynamics caused the drying problem for three of the RCMs. Errors in the atmospheric dynamics may lead to erroneous moisture transport towards Central Europe and hence cause or enhance the summer drying problem. However, the moisture transport is also affected by the convective moisture supply from land and ocean areas.

Soil moisture controls the partitioning of the available energy into latent and sensible heat fluxes and conditions the amount of surface runoff. This factor links the energy, water and carbon fluxes by controlling evapotranspiration (Koster et al. 2004; Dirmeyer et al. 2006; Seneviratne and Stöckli 2008). Seneviratne et al. (2006) specifically highlighted the importance of soil-moisture–temperature feedbacks (in addition to soil-moisture–precipitation feedbacks, as mentioned above) for future climate changes in Central and Eastern Europe. A comprehensive review on soil moisture feedbacks was provided by Seneviratne et al. (2010). Thus, land surface effects on precipitation have already been investigated in detail for various scales, such as the influence of small-scale land-air energy and mass fluxes by Larsen et al. (2016) and Shrestha et al. (2014). Anders and Rockel (2009) showed the effect of prescribed soil types on the climate over south-eastern Europe. However, coupling effects from the remote ocean (i.e., air sea coupling) and their effects on land are poorly understood. The RCMs that were used in the above studies were basically atmosphere-only models, and air-sea interactions were not considered, so remote effects from air sea coupling were neglected in this specific context. In our study, we address overly weak large-scale moisture convergences from adjacent ocean/seas as a possible reason for the RCM summer drying problem over Central Europe. We also investigate whether the coupling of an atmospheric RCM with an ocean model that covers the North Sea and the Baltic Sea may lead to an improved simulation of moisture convergence and a subsequent reduction in the dry bias.

Previously, dry biases in models were primarily recognised by the monthly or annual mean precipitation. However, averaging over time creates a smoothing effect on the differences between the model results and observations, which increases the difficulty of discerning the underlying causes of the differences. This study provides an analysis of summer dry biases over Central Europe from two RCMs over various timescales from seasonal and monthly to short extreme events. Moreover, summer heavy rainfall that causes extreme events over Central Europe is analysed under specific weather conditions. The precipitation characteristics of a particular terrestrial region are determined by the atmospheric moisture supply from various source regions (e.g., van der Ent et al. 2010; Gimeno et al. 2010). Larger precipitation amounts are observed when the atmospheric circulation favours more direct links to the source. We suppose that the coupling effect of the North Sea and the Baltic Sea on precipitation over Central Europe would be

pronounced under a specific weather condition in which a certain weather pattern is dominant and the sea-to-land moisture flow would persist. The new point of this study is that we analyse the performance of the various RCM simulations for different categories of so-called "weather regimes" (James 2006, 2007). Weather regimes are determined using the "Grosswetterlagen" (GWL) catalogue classification system, which is maintained by the German Weather Service (DWD) and extends from 1881 to the present. Twenty-nine single Hess and Brezowsky Grosswetterlagen (HB-GWL) regimes (e.g., Cyclonic Westerly WZ, Trough over Central Europe TRM, Trough over Western Europe TRW) and six circulation types (i.e., Westerly, Northerly, Easterly, Southerly, Cyclonic and Anticyclonic) have been classified based on common features of single regimes (James 2007). In our study, the six circulation types, particularly the Northerly Circulation, is considered to identify potential teleconnections between the changes in sea surface temperature (SST) over the coupling domain (i.e., the North Sea and the Baltic Sea) and the changes in precipitation over the areas of continental Central Europe that are distally located from the coupling domain.

The article is structured as follows: Section 2 describes the models and data that are used to analyse the dry bias; Section 3 provides an analysis of the models' dry bias in terms of the summer mean, weather regimes and extreme precipitation; and Section 4 includes a discussion and our conclusions.

2 Models and data

Simulations of RCMs and AORCMs that have been produced within the CLM-Community (Climate Limited area Modeling Community, www.clm-community.eu) and the Swedish Meteorological and Hydrological Institute (SMHI) are described in Sections 2.1 and 2.2, respectively. These simulations were conducted independently of each other by the respective modelling groups; therefore, the configurations of the CCLM and RCA4 simulations differ in terms of their resolution and coupling domain. An overview of the models and simulation data that are analysed in this study is provided in Table 1. Section 2.3 lists the reanalysis and observation data that are used for the evaluation.

2.1 CCLM simulations

Two versions of the atmospheric model CCLM (Rockel et al. 2008) cosmo4.8_clm19 (CCLM 4.8) and cosmo5.0_clm6 (CCLM 5.0) were used in this study as the stand-alone atmospheric model and a component of an air-sea coupled system model. An atmosphere-only experiment that used CCLM 4.8 (denoted by UNCPL_HZG) was configured with a horizontal grid mesh size of 0.44° (approximately 50 km), 40 vertical atmosphere layers in rotated coordinates and a time step of 300 s over the EURO-CORDEX (Coordinated Regional Climate Downscaling Experiment, Giorgi et al. 2009) domain for the period of 1979–2009. Here, CCLM uses the 6-h ERA-interim reanalysis data (Dee et al. 2011; denoted by ERA-Int) as initial and boundary conditions with a sponge zone of 10 grid points. The occurrence of sea ice in CCLM is deduced according to the skin temperature (below -1.7 °C, sea ice is assumed). Sea ice is considered only with respect to its albedo and surface roughness length. The surface height and orographic roughness length were obtained from the Distributed Active Archive Center's gtopo30 dataset (U.S. Geological Survey 2004). The land-sea fraction, vegetation parameters (leaf area, root depth, etc.) and lake fraction were derived from the Global Ecosystems V2.0 dataset. The soil type was obtained from the Food and Agriculture Organization of the United Nations (FAO). The climatological deep soil temperature was provided by the Climate Research Unit (CRU; University of East Anglia, Harris et al. 2013). Land surface processes, such as the heat and water transport in soil and the freezing and melting of soil water and ice, are parameterised using the TERRA-ML scheme (Schrodin and Heise 2001; Doms et al. 2011), and cumulus convection is parameterised using the Tiedtke scheme (Tiedtke 1989).

The coupled experiment CPL_HZG is configured with the coupled system COSTRICE using the same configuration as the UNCPL_HZG. COSTRICE includes the ocean model TRIMNP v2.5 (Casulli and Cattani 1994; Casulli and

Stelling 1998; Ho-Hagemann et al. 2013, 2015) and the sea ice model CICE v5.0 (Hunke et al. 2013), which are coupled via the coupler OASIS3-MCT v2.0 (Valcke et al. 2013). COSTRICE is designed to run in parallel on the supercomputing system at the German Climate Computing Centre (DKRZ). TRIMNP is configured with a 12.8-km horizontal grid mesh size and 50 vertical ocean levels to cover the Baltic and North Seas and a part of the North Atlantic Ocean, which is bounded by Iceland to the north and the Bay of Biscay to the south. The initial and boundary conditions of TRIMNP are updated using ECMWF ORAS4 monthly reanalysis data (Balmaseda et al. 2013). The original global CICE model is set up as a regional version (Ho-Hagemann et al. 2013) with the same horizontal grid as TRIMNP to reduce the computing time, but the domain covers only the Baltic Sea and Kattegat, which is a part of the North Sea (Fig. 1, the light-blue area). CICE calculates five categories of ice and uses the new thermodynamics option "mushy" formulation (Turner et al. 2013). The standard thermal conductivity option that is used is 'MU71' following Untersteiner (1964) and Maykut and Untersteiner (1971). The revised Elastic Viscous Plastic (EVP) sea ice rheology and the upwind advection algorithm are applied in this study (see more details in Hewitt et al. 2011). The initial conditions of CICE are determined using NOAA's Optimum Interpolation Sea Surface Temperature dataset OISSTv2 SST (Reynolds et al. 2007). TRIMNP and CICE both perform calculations at a time step of 240 s. The integration domain of the models is shown in Fig. 1. The coupling time step between the components is 1 h. TRIMNP is driven by the mean sea level pressure, total precipitation, surface net shortwave radiation, longwave downward radiation, and sensible and latent heat fluxes from CCLM. In addition to the radiation and heat fluxes, CICE requires information on the temperature, wind velocity, specific humidity, air density (at the lowest vertical model level of CCLM), cloud cover, and rain and snow rates for use as atmospheric forcing. Outgoing longwave radiation from the sea/ice surface is calculated in TRIMNP and CICE according to the surface temperatures. Over the air-sea coupling domain, which covers the Baltic Sea, the eastern region of the North Sea and a part of the North Atlantic Ocean, CCLM receives skin temperatures, which are the combination of the SST from TRIMNP and the sea ice skin temperature from CICE, weighted by the sea ice concentration (Ho-Hagemann et al. 2013, 2015). The SST over the north-western part of the North Sea along the British coastline and the western boundary area of TRIMNP is not passed to CCLM because of the large SST bias, which may be associated with the short spin-up time (5 years) of the ocean model. The ERA-Int SSTs are used for these non-matching areas between the domains of CCLM and TRIMNP. The coupled ocean domain of the COSTRICE coupled system covers the Baltic Sea and North Sea, which is similar to other coupled systems (e.g., Pham et al. 2014; Dieterich et al. 2013; Wang et al. 2015), and a part of the North Atlantic Ocean. We expect that the larger coupling domain may cause a more pronounced coupling effect on the precipitation simulations.

A variant of CCLM 4.8 (cosmo4.8_clm11) was used to generate the coastDat2 dataset (Geyer 2014) for a domain that covered Europe and adjacent seas and includes a slight northward shift compared to the information in Fig. 1 at a spatial grid size of 0.22^{o} (approximately 24 km) on rotated coordinates with a 150-s time step. Forty vertical atmosphere levels up to a height of 27 km were used, with a higher resolution at the lower boundary. The meteorological initial and boundary conditions were obtained from the 6-hourly NCEP1 reanalysis data composites (Kalnay et al. 1996; Kistler et al. 2001), and the spectral nudging technique of von Storch et al. (2000) was applied every fifth time step. Similar physical parameterisations to that of UNCPL_HZG and CPL_HZG were configured. First, the model was run for the period from 1948 to 1952 as a spin-up time to determine the soil moisture. Then, a continuous simulation was restarted at 1948 with the obtained soil moisture values (Geyer 2014). The precipitation values from the coastDat2 dataset were used for a comparison with the UNCPL_HZG and CPL_HZG experiments.

CCLM 4.8 was set up to run on the Blizzard system (consisting of IBM CPUs) at DKRZ until September 2015, when DKRZ was moved to the Mistral system (consisting of Intel Xeon CPUs). Since this time, the newest version of

CCLM (5.0) was installed on the Mistral system to replace the older version 4.8. CCLM version 5.0_clm6 includes several changes in the dynamics and physics compared to version 4.8 (Table 2). Otherwise, the setup of CCLM 5.0 was similar to those of UNCPL_HZG, CPL_HZG and coastDat2. The uncoupled and coupled experiments of CCLM 5.0 that were used in the comparison are denoted by UNCPL_HZGv5 and CPL_HZGv5 with the suffixes "_044" and "_022" for two resolutions of 0.44º and 0.22º, respectively. For both resolutions, the CCLM 5.0 experiments used ERA-Int data as initial and boundary conditions, similar to CCLM 4.8. The time steps for the runs on the 0.44º and 0.22º grids were 300 s and 150 s, respectively.

Higher resolution provides better results for precipitation patterns and daily precipitation intensity, particularly for regions with distinct orography (Boberg et al. 2010). A resolution of 50 km, which is not high for simulations of orographically induced precipitation and local circulation (Giorgi 2006), was used in this study for CCLM for two major reasons. First, when the CCLM 4.8 experiments were performed on the Blizzard system, increasing CCLM's resolution in the coupled model COSTRICE 4.8 for long-term simulations was difficult because the computing resources were limited. Second, extreme precipitation was considered with respect to the 90th percentile of the area-averaged precipitation of Central Europe (excluding the Alps; see Fig. 1), where the orography is not overly pronounced. The distribution of heavy precipitation over a relatively large area from large-scale moisture convergence was considered with this resolution. Later on, the coupled model of CCLM 5.0 was set up to run on both the 0.44º (approximately 50 km) and 0.22º grids (approximately 24 km) because more computing and storage resources were available on the Mistral system.

Several sensitivity experiments were conducted with CCLM 4.8 and CCLM 5.0 to obtain more robust results. A sensitivity test was performed on CCLM 4.8 with a smaller sponge zone (4 points instead of 10 points) to add more noise to the CCLM domain that was imposed by the less smooth transition from the lateral boundaries to the CCLM-generated dynamics within the domain. The uncoupled and coupled simulations of this sensitivity test are denoted by UNCPL_HZG_rlwidth and CPL_HZG _rlwidth. A sensitivity test of UNCPL_HZGv5_044, CPL_HZGv5_044 used some similar parameter values (i.e., rlam_heat, tkhmin and tkmmin, see Table 2) to the setup of CCLM 4.8 and had the suffix "_conf4.8". The experiments UNCPL_HZGv5_044, CPL_HZGv5_044 and UNCPL_HZGv5_022, CPL_HZGv5_022 used the new initial soil depth values of the ERA-Int data (0.035, 0.175, 0.64 and 1.775 m), which have been updated since August 2016 to replace the old values (0.015, 0.1, 0.405 and 1.205 m, respectively). A sensitivity test of UNCPL_HZGv5_022, CPL_HZGv5_022 with the old initial soil depth values had the suffix "_oldsoil". All the CCLM 4.8 experiments also used the old values. These sensitivity experiments are listed in Table 1.

2.2 RCA4 simulations

Uncoupled and coupled simulations were conducted at SMHI with the recently developed regional model NEMO-Nordic for the North Sea and the Baltic Sea. These simulations were described in detail by Gröger et al. (2015).

The atmospheric component was the Rossby Centre regional Atmospheric climate model (RCA, Samuelsson et al. 2011; Wang et al. 2015). The current version (RCA4) of the model has undergone modifications as described by Kupiainen et al. (2014). The RCA4 model also covers the EURO-CORDEX domain with a slight shift of the western boundary to the east (see Gröger et al. 2015, Fig. 1b). The model was configured with 40 vertical terrain-following levels and a horizontal resolution of 0.22º (approximately 24 km). The global database ECOCLIMAP (Champeaux et al. 2005) for soil and ecosystems was used in RCA4 to represent the land surface properties. The surface characteristics of the coupled area that were simulated by the ocean model (SST, sea ice fraction, ice albedo and temperature) were communicated to RCA4 via the OASIS3 coupler (Valcke et al. 2013). The atmosphere-ocean coupling time step was

3 h. In stand-alone runs, the SSTs were obtained from ERA40 reanalysis data (Uppala et al. 2005).

The ocean component used the Nucleus for European Modelling of the Ocean (NEMO, Madec 2008) version 3.3, which was configured for the North Sea and the Baltic Sea at a horizontal resolution of two nautical miles (approximately 3.7 km). The model domain restricted the North Sea to a northern boundary of 60° N, although the domain covers the entire Baltic Sea. The water column was subdivided by 56 unevenly spaced levels. The first model layer was approximately 3 m thick. NEMO was forced by wind stresses, radiative heat fluxes, P-E (precipitation minus evaporation), and sea-level pressure when coupled interactively to RCA4. NEMO version 3.3 also contained the sea ice model LIM3, which includes a representation of dynamic and thermodynamic processes (for details, see Vancoppenolle et al. 2009).

The uncoupled and coupled RCA4 experiments are hereafter denoted by UNCPL_SMHI and CPL_SMHI. The available data for the RCA4 experiments were compared with the CCLM experiments in this study. In Section 3, the simulated air temperature at a height of 2 m (T_2M), surface temperature (T_S) or SST over the ocean, MSLP, wind components and precipitation of the experiments are analysed and compared with the observational data in detail.

2.3 Observations

The NOAA High-resolution Blended Analysis SST daily data (OISSTv2) on a 0.25° global grid (provided by the NOAA/OAR/ESRL PSD, Boulder, Colorado, USA from their website at http://www.esrl.noaa.gov/psd/data/gridded/data.noaa.oisst.v2.highres.html) were collected and then compared to the SSTs of the experiments. OISSTv2 is one of the highest spatial-resolution SST products on a global grid that are currently available. The dataset is a combination of ocean temperature observations from satellite and in situ platforms (i.e., ships and buoys).

The simulated MSLP and T_S over land in the experiments were compared to the ERA-Int reanalysis data on the approximately 0.75° grid, whereas the T_2M and precipitation over land were compared to the most recent version 13.1 of the E-OBS data on the 0.22° grid (Haylock et al. 2008). E-OBS covers the entire European land surface and is based on the European Climate Assessment and Dataset (ECA&D) station dataset and data from more than 2000 additional stations from different archives. The analysis and observation data and the experimental results were interpolated onto the CCLM grid (0.44° or 0.22°) for comparison.

3 Results

In Section 3.1, the long-term averages of the summer precipitation, T_2M, MSLP and SST are analysed for the CCLM 4.8 and SMHI simulations for the period of 1986–2009. Then, an analysis of the precipitation for different weather regimes is provided in Section 3.2. All the figures in these two sections and in Appendix A are limited to the considered area - Central Europe. The results of the uncoupled and coupled CCLM 5.0 experiments are very similar and thus are not shown in these two sections. In Section 3.3, extreme precipitation is considered in terms of very wet days under Northerly Circulation Type conditions. In this section, CCLM 4.8 and CCLM 5.0 simulations are considered, including different sensitivity tests (Table 1), which are analysed together with the SMHI simulations to obtain more robust conclusions.

3.1 Long-term average

Mean sea level pressure

The ERA-Int MSLP data (Fig. 2a, left panel) show that European weather during summer was dominated by the Icelandic low in the north-western corner of the EURO-CORDEX domain and the Azores High over the Atlantic Ocean in the south-western corner. This MSLP distribution is a typical NAO-like pattern. Low-pressure areas were also found

over the Mediterranean Sea, particularly in the eastern region, and over northern Europe. This MSLP pattern was well reproduced by the experiments (Fig. 2a), with positive biases of 0.5–1.0 hPa in the CCLM simulations over the North Atlantic Ocean and positive biases of 0.5–1.5 hPa in the RCA4 simulations over Scandinavia. Over the Mediterranean Sea, the CCLM simulations tended to underestimate the MSLP by 2.0–3.0 hPa, whereas the RCA4 simulations overestimated the MSLP by 1.0–1.5 hPa (not shown). The difference in the MSLP between CCLM and RCA4 may have been related to their different forcings (ERA-Int and ERA-40). In both systems, the MSLP of the coupled model was generally similar to that of the atmosphere-only run.

Air temperature at 2 m

Fig. 2b shows the summer mean E-OBS T_2M (left panel) and the differences in the model results compared to the E-OBS data. During summer, a large temperature gradient (approximately 10 ºC) occurred between northern and southern Europe. In the warm climate of southern Europe, however, the Alpine area had a relatively cold temperature because of the high orography. All the experiments show pronounced cold biases in northern Europe, which supports the results of Kotlarski et al. (2014). Over Scandinavia, the cold bias of the SMHI was 1–2 ºC more pronounced than that of CCLM. In southern Europe, the SMHI reproduced T_2M rather well, whereas CCLM showed a large warm bias of 2–3 °C. Similar to the MSLP case, the coupled and uncoupled T_2M results were relatively similar in both models.

Sea surface temperature

The OISSTv2 data (Fig. 2c, left panel) showed a cold pool to the north (e.g., approximately 8–13 °C in the North Atlantic Ocean, the North Sea and the Baltic Sea) and a warm pool to the south (e.g., approximately 23–27 °C in the tropical Atlantic Ocean and the Mediterranean Sea, not shown) of the EURO-CORDEX domain.

Compared to the OISSTv2 data, the ERA-Int reanalysis data (the forcing of the CCLM simulations) were 0.2–1 °C warmer and the ERA-40 reanalysis data (the forcing of the SMHI simulations) were 0.2–1 °C colder over most areas of the open ocean, except for a warmer area of 1–2 °C over the eastern Mediterranean Sea. Along the coastlines, the ERA-Int SST and ERA-40 SST were often higher than the OISSTv2 data, which may have been associated with the inconsistencies of land sea masks between the SST observations and simulations from the interpolation. Overall, the ERA-Int SST was approximately 0.5 °C higher than the ERA-40 SST. These different forcings and SSTs of CCLM and RCA4 may have affected the performance of the atmosphere-only simulations.

Over the CCLM coupling areas, the SST of the CPL_HZG was similar to that of UNCPL_HZG/ERA-Int, although slightly colder over the North Sea and the Baltic Proper and warmer over the Bothnian Bay. Over the RCA4 coupling areas, the SST of CPL_SMHI was approximately 1–2 ºC warmer than that of UNCPL_SMHI (ERA40) (see Figs. 6 and 8 in Gröger et al. 2015). Nevertheless, the summer mean T_2M of CPL_SMHI and UNCPL_SMHI were mostly identical (Fig. 2b). Both coupled experiments for CCLM and RCA4 had warm SST biases over Bothnian Bay, although the reason for this phenomenon remains unclear.

Precipitation

The E-OBS data for summer precipitation (Fig. 2d, left panel) showed a vast wet region with precipitation amounts of 2–4 mm/day within northern Europe and Central Europe, particularly over the Alpine area (which could be more than 6 mm/day) because of the orography-caused uplifting effect, and a dry sub-tropical region with monthly precipitation amount of less than 1 mm/day within southern Europe around the Mediterranean Sea (not shown).

Compared to the E-OBS data, CCLM had wet and dry biases in northern and southern Europe, respectively, a clear N-S pattern. This phenomenon may have been related to the stronger simulations of the Azores High over the Atlantic

Ocean by CCLM, which caused a more pronounced North Atlantic oscillation (NAO) and stimulated wet Atlantic air masses to move into and generate more precipitation in the northern regions, with less precipitation generated further south. The wet bias over northern Europe might have caused a cold bias (Fig. 2b). Over southern Europe, T_2M was too high and the precipitation was too low. This phenomenon can be explained by a shortage of cloud cover, which allowed more incoming shortwave radiation to reach the area. Additionally, a shortage of precipitation may have created a shortage of evapotranspiration, which led to the release of less latent heat. Hence, the surface and the air near the surface were too warm.

The warm and dry summer biases over southern Europe are consistent with previous findings (e.g., Hagemann et al. 2004 for PRUDENCE; Christensen et al. 2008 for ENSEMBLES; and Kotlarski et al. 2014 for CORDEX). Kotlarski et al. (2014) focused on the underestimation of summertime precipitation and soil moisture-temperature coupling because low soil moisture contents, which can occur under precipitation deficits, limit the amount of energy that is used for the latent heat flux in soil moisture-controlled evaporative regimes, thereby increasing the sensible heat flux and ultimately increasing the air temperature (e.g., Seneviratne et al. 2010). This feedback is sensitive to all processes that interfere with the regional balance of water and energy, including land-surface, boundary layer, convective and radiative processes.

The RCA4 simulations presented a dry bias only over the Danube region and overestimated wet conditions elsewhere. The overall wet bias of RCA4 may have created the cold bias in T_2M (Fig. 2b). Generally, large differences were not observed between the coupled and uncoupled runs of both model systems, which is consistent with the results of Gröger et al. (2015). The annual and seasonal precipitation and T_2M biases when averaged over Central Europe in the experiments were similar to what was observed by Kotlarski et al. (2014). These authors noted that certain bias characteristics, such as a predominant cold and wet bias in most seasons over most of Europe and a warm and dry summer bias over southern and south-eastern Europe, reflect the common model biases of many other models.

Table 3 shows the long-term mean and the 90th and 95th percentiles (*PC90* and *PC95*, respectively) of the daily summer (JJA) precipitation area when averaged over Central Europe (the area bound by the red rectangle in Fig. 1) for 1986–2009. The *Mean* column shows that the CCLM and RCA4 experiments generally had dry and wet biases, respectively, compared to the E-OBS data. The CPL_HZG and the coastDat2 data were similar and provided more accurate results than UNCPL_HZG. The *PC90* and *PC95* columns provided information on the extreme values, which behaved similarly to the mean values, except for those of the coastDat2 data, which presented the smallest *PC90* and *PC95*. The *PC90* values of the E-OBS and the models were approximately 5–6 mm/day. The probability distribution function (PDF) of the coupled experiments of both CCLM and RCA4 was slightly better than that of the uncoupled experiments, particularly for precipitation that was greater than 7 mm/day.

In the next section, the performance of the experiments is analysed in more detail with respect to the weather regimes, with a focus on the differences between the coupled and uncoupled experiments of CCLM and RCA4.

3.2 Weather regimes

In this section, we analyse the performance of the different experiments under specific weather regimes, i.e., the six major circulation types that were classified according to James (2007; see Section 1). Our primary focus is on the Northerly Circulation Type because the airflow for this type originates from the North Atlantic Ocean, passes the coupling areas and causes moisture advection within Central Europe.

First, the DWD weather regime data are used to categorise the daily data that were recorded from 1986 to 2009 into the six circulation types. Daily data that present an undefined GWL are excluded from the analysis. Second, the E-OBS and modelled data that correspond to each category are further considered in two cases: all days and very wet days. The

"all days" term refers to the entire investigated daily rainfall time series for JJA from 1986 to 2009. In total, 2194 "all days" are detected. The "very wet days" term refers to days when the area-averaged precipitation of Central Europe is equal to or greater than 5 mm/day (approximately equal to the *PC90* of the E-OBS and modelled data). In total, 345 "very wet days" are detected.

For the "all days" case, the RCA4 experiments presented obvious wet biases, and UNCPL_SMHI and CPL_SHMI were similar (not shown). The CCLM experiments underestimated the precipitation for all circulation types. CPL_HZG and UNCPL_HZG were not clearly different in this case. Among all the CCLM experiments, a small dry bias was observed for the Easterly and Anticyclonic regimes because of the low precipitation that was observed for these circulation types.

For the "very wet days" case (Fig. 3), all the models presented a dry bias compared to the E-OBS data for the six circulation types. In the E-OBS data, the Northerly Circulation Type prevailed on 98 days of the 345 very wet days and had the highest average heavy precipitation value (8 mm/day) over Central Europe, whereas the other circulation types had 7–7.5 mm/day. The RCA4 simulations presented the best performance and underestimated the precipitation amount by approximately 1–2 mm/day; these simulations were followed by those of coastDat2, CPL_HZG and UNCPL_HZG. The coupled and uncoupled experiments of RCA4 behaved almost identically. However, for the CCLM simulations, CPL_HZG presented an improvement in the dry bias compared to UNCPL_HZG, particularly for the Northerly Circulation Type, in which the dry bias was reduced by approximately 1 mm/day. The highest precipitation of CPL_HZG was associated with the Northerly Circulation Type, which was similar to the E-OBS data and the other experiments; however, the maximum precipitation of UNCPL_HZG was associated with the Southerly Circulation Type.

The mean biases of the MSLP, SST and precipitation for the very wet days of the Northerly Circulation Type are displayed in Fig. 4, in the same manner as in Fig. 2. In UNCPL_HZG, the Azores High appeared to extend too far to the east (Fig. 4a), which might have suppressed heavy precipitation over Central Europe (Fig. 4c). These biases were reduced in CPL_HZG. However, the MSLP and precipitation simulations of RCA4 and RCA4-NEMO were not remarkably different. The behaviour of the SSTs (Fig. 4b) was relatively similar to that in Fig. 2c, although the biases over the coupling domain were 0.2–0.4 ^{o}C more negative, except in UNCPL_HZG. The precipitation bias (Fig. 4c) had a similar pattern as in Fig. 2d, although with larger values. However, the dry bias over Central Europe in UNCPL_HZG was reduced by 10% on average over all of Central Europe, by up to 38% over Poland and by up to 30% over Germany in CPL_HZG compared to the E-OBS data, which is consistent with the results in Fig. 3. The larger area of moisture convergence over Central Europe on days that exhibited the Northerly Circulation Type as reproduced by CPL_HZG compared to what was reproduced by UNCPL_HZG may explain the reduced precipitation bias (figure not shown). Hence, the CPL_HZG experiment provided colder SSTs over the North Sea and the Baltic Sea, which produced a less positive MSLP bias over Central Europe and a reduced dry bias because of the heavy rainfall.

However, several questions can be raised concerning the robustness of the results:

1. Did the SSTs of the coupled systems present a systematic cold or warm bias compared to the forcing SST that was used in the uncoupled model, particularly for the very wet days of the Northerly Circulation Type?

2. How did changes in the SST over the North Sea and the Baltic Sea change heavy precipitation over terrestrial areas of Central Europe?

3. Was the difference in heavy precipitation between CPL_HZG and UNCPL_HZG statistically significant?

To answer the first question, we analysed the 98 very wet days of the Northerly Circulation Type for cases with colder or warmer North Sea conditions (i.e., the SST of CPL_HZG over the North Sea was lower or higher than that of

UNCPL, respectively). The Baltic Sea was not considered in this analysis because the SSTs of CPL_HZG were always lower than those of UNCPL_HZG over the Baltic Sea and the SSTs of CPL_SMHI were always higher than those of UNCPL_SMHI. CCLM had 69 days with colder North Sea conditions and 29 days with warmer North Sea conditions (Fig. 5a), whereas RCA4 had 34 and 64 days, respectively (Fig. 6a). Obviously, the coupled systems did not always provide warmer or colder North Sea conditions relative to the forcing SSTs; however, CPL_HZG tended to reduce the SSTs at a frequency of approximately 70% (69/98 days) and CPL_SMHI tended to increase the SSTs at a frequency of approximately 65% (64/98 days). The SST forcing of CCLM was warmer than the OISSTv2 data, and the SST forcing of RCA4 was colder. Thus, the coupled systems appeared to produce SSTs that were closer to the OISSTv2 data.

A common result of the CCLM and RCA4 simulations was that the SSTs of the North Sea influenced the T_S of Central Europe, particularly on very wet days of the Northerly Circulation Type (Fig. 5a and Fig. 6a). As the North Sea became colder, so did Central Europe, and vice versa, and this effect spread further southeast of the domain, which is consistent with the findings of Pham et al. (2014). Hence, we propose that the changes in the SST and the associated effects on the T_S over remote continental Central Europe that were caused by coupling are a common feature among the models, i.e., a robust result.

The answer for the second question regarding CCLM can be obtained from the information in Fig. 5 and Appendix A (denoted by App. A). During the colder North Sea days, the wind flow from the North Atlantic Ocean that passed from the North Sea to Central Europe was more intense in CPL_HZG than in UNCPL_HZG. This finding is surprising because cooler SSTs should stabilise the atmosphere and thus promote weaker winds, which was recently found for the winter season (Gröger et al. 2015). However, when the T_S over Central Europe was higher than the SSTs in the North Sea (Fig. 5a), the wind from the ocean to the land sometimes sped up (Fig. 5b) because wind tends to converge from cold surfaces to warm surfaces to support vertical updraft. The stronger wind over the North Sea then generated a larger latent heat flux from the ocean to the atmosphere (App. Af), and intensified the low over Central Europe and the North Sea (App. Aa), which both support the moisture convergence from the North Sea to Central Europe (App. Ad). Consequently, a larger amount of precipitation fell over Central Europe in CPL_HZG than in UNCPL_HZG (Fig. 5d). This larger precipitation cooled down the T_S over Central Europe, which decreased the sensible heat flux (App. Ae) and created a cooler T_2M (App. Ab). The cooler T_S over Central Europe also caused less evaporation and therefore less latent heat flux (App. Af), which was sometimes followed by an increase in the latent heat flux because of the increased evapotranspiration over the wet soil moisture area after precipitation. The diagram in Fig. 7 is a summary of these interactions and the feedback loop. This diagram is partly based on a study by Bender et al. (1993), although these authors focused on strong air-sea interactions and feedback under conditions with tropical cyclones and hurricanes.

The answer to the third question, which is related to the statistical significance of the differences in heavy precipitation between CPL_HZG and UNCPL_HZG, is addressed in the following. These significances were calculated for both CCLM and RCA4 using the Students *t-test*. The *PC90* values were used to determine the heavy rainfall time series for each grid point for the E-OBS data and for the experiments. Fig. 8a and b show the *t-test* results for grid points for which the number of rainfall days was greater than 10% of the total days of the entire time series (i.e., 2208 days) and the Northerly Circulation Type (i.e., 553 days), respectively.

Fig. 8 clearly shows that interactive coupling led to wetter conditions over Central Europe, the North Sea and the Baltic Sea and significantly diminished the dry bias in this area for CCLM. For RCA4, a small change was observed to the south of the North Sea and within the Baltic catchment, but significant changes were not observed at greater distances from the coupling area. The coupling effect under the Northerly Circulation Type was more remarkable (Fig. 8b), particularly in CCLM. For this Northerly Circulation Type, the effect in RCA4 was very small in Central Europe

but rather pronounced over Finland. A potential reason for the weak coupling effect in RCA4_NEMO is that the time-by-time (e.g., 3 h) changes in the SST in NEMO were smaller than those in TRIMNP, particularly over the coupled North Sea. The standard deviations of the 3-h SST data over the North Sea in NEMO and TRIMNP were approximately 2.5 and 3 °C, respectively. The differences in the SST's standard deviations between the coupled and uncoupled cases for RCA4 and CCLM were approximately 0.3 and 0.8 °C, respectively. This result implies that the coupled North Sea was more actively responding to atmospheric forcing in TRIMNP than in NEMO, which may have caused a stronger feedback from the sea in CCLM than in RCA4. However, over the Bothnian Bay and Bothnian Sea, the SST standard deviation in NEMO was larger than the forcing SST in ERA-40, which may partly explain the significant differences in precipitation over Finland between RCA4_NEMO and RCA4 (Fig. 8b). However, these assessments should be further investigated in the future.

3.3 Extreme precipitation

The extreme precipitation that was observed in this section is the daily precipitation when averaged over Central Europe on the very wet days (cf. Section 3.2) under Northerly Circulation Type conditions. The 98 very wet days of the Northerly Circulation Type for the E-OBS data were used to construct sets of data for the experiments. The results are shown in Fig. 9. The coupled model CCLM 4.8 in the standard set up and the sponge zone width sensitivity test appeared to have better heavy precipitation than the uncoupled CCLM, especially for the Oder and Elbe flood events (Fig. 9a and b). The stand-alone CCLM 4.8 with a smaller sponge zone width often had a larger dry bias than the standard CCLM 4.8, which was most pronounced during the Oder flood event (not shown). However, the coupled and uncoupled CCLM 4.8 had a large dry bias compared to the E-OBS data, which is consistent with the above analysis. The coupled and uncoupled SMHI simulations were very similar (Fig. 9c), which was also the case for CCLM 5.0 (Fig. 9d and e). CCLM 5.0 was not strongly sensitive to the initial condition of the soil depth and several considered physical parameters at both resolutions of 0.44° and 0.22° (not shown). CCLM 5.0 reproduced slightly better extreme events on the 0.22° grid (Fig. 9e) than on the 0.44° grid (Fig. 9d). The ensemble mean of all the CCLM 4.8, CCLM 5.0 and SMHI simulations in Fig. 9f indicates that mostly the coupled model was closer to the E-OBS data than the uncoupled model, especially for extreme rainfall events, but the improvement was rather small.

An overview on the daily precipitation bias for all members of the ensemble is provided in Fig. 10, in which the range of the minimum and maximum biases of the ensemble uncoupled and coupled experiments compared to the E-OBS data are expressed by the shaded areas and the ensemble mean biases by the solid lines. The results with (Fig. 10a) and without (Fig. 10b) the SMHI simulations are similar, with a general dry bias of 5 mm/day and up to 12 mm/day and 10 mm/day for the Oder and Elbe flood events, respectively. The shaded area of the uncoupled models tends to cover larger dry biases than the coupled models, which is most pronounced in these specific flood events. The mean biases of the uncoupled and coupled models show a similar result as in Fig. 9f. These results are confirmed by the statistical scores (mean error ME, mean absolute error MAE, root mean squared error RMSE and correlation coefficient Corr.) of the ensemble mean of the uncoupled (UNCPL) and coupled (CPL) experiments against the E-OBS data, which are shown in Table 4. All the scores of the coupled models are better than the uncoupled models both when including and excluding the SMHI simulations, but the difference between the scores of the coupled models and uncoupled models is not very large.

4 Discussion and conclusions

In this study, we investigated whether using coupled atmosphere-ocean systems can reduce the summer dry bias of regional climate models over Central Europe. Simulations of two RCMs (CCLM and RCA4) in stand-alone and coupled modes were analysed in terms of long-term summer mean values over 30 years (1979–2009), weather regimes (focusing

485 on the Northerly Circulation Type), and extreme rainfall events.

486 Comparisons of the coupled systems with the atmosphere-only models showed that coupling provided varying
487 effects over the considered timescales. In terms of the long-term seasonal means, the coupled and uncoupled
488 simulations were mostly identical, which was the case for CCLM and RCA4. However, if extreme precipitation events
489 were considered, particularly under the Northerly Circulation Type regime, when the airflow from the North Atlantic
490 Ocean passed the coupling domain over the North Sea, the simulations of COSTRICE 4.8 were generally more accurate
491 than the atmosphere-only CCLM 4.8. Here, COSTRICE 4.8 provided an average reduction in the dry bias for heavy
492 precipitation (exceeding the 90th percentile) of approximately 10% over Central Europe compared to CCLM 4.8, and
493 the dry bias reduction increased to 38% over Poland and 30% over Germany. The benefit of coupling with COSTRICE
494 4.8 was that the air-sea feedback (e.g., wind-evaporation-sea surface temperature) and land-sea interactions were better
495 reproduced, which improved the large-scale moisture convergence from the sea to the land. Increased wind speeds over
496 the sea increased the evaporation rates and latent heat energy, which further increased the wind speeds; however,
497 intensified turbulent mixing at the sea surface from this increased wind speed generated mixed layer deepening and
498 surface cooling (Bender et al. 1993). This sea surface cooling increased the contrast between the land and sea
499 temperatures, and this effect, together with the increasing wind speed over the sea, intensified the large-scale moisture
500 convergence from the North Atlantic Ocean to Central Europe in the COSTRICE model, particularly under Northerly
501 Circulation Type conditions in summer. However, the effects of the air-sea coupling for RCA4 and CCLM 5.7 were
502 unclear inland. The precipitation difference between RCA4 and RCA4-NEMO over Central Europe was statistically
503 insignificant for heavy precipitation, which is consistent with the results of Gröger et al. (2015). The results were
504 similar for CCLM 5.0. The summer dry bias was not very large in the stand-alone RCA4 and CCLM 5.0 simulations,
505 and the coupling had no room to improve the dry bias. The coupling may have had a beneficial effect only if the
506 atmosphere-only model, such as CCLM 4.8, had a poor performance in reproducing the summer precipitation over
507 Central Europe because of the excessively weak large-scale moisture convergence from the nearby ocean/seas. This
508 poor performance of CCLM 4.8 was also apparent in the coastDat2 simulation (Fig. 3) despite the higher resolution
509 (0.22^{o}) and the spectral nudging technique that was applied in coastDat2.

510 In addition, the different behaviours of CCLM 4.8 and the other two RCMs (RCA4 and CCLM 5.0) may have been
511 related to 1) the different sensitivities of the atmospheric model components to changes in the SST over the coupling
512 domain or 2) the size and exact location of the coupling domain. First, sensitivity tests of CCLM 4.8 and CCLM 5.0
513 showed that CCLM 5.0 provided rather stable results but CCLM 4.8 was sensitive to changes in the sponge zone width.
514 The changes in the dynamics and physics of CCLM 5.0 improved the summer precipitation and decreased the very large
515 positive bias in the winter mean sea level pressure in CCLM 4.8 (not shown). Thus, the older CCLM 4.8 may have
516 simulated a regional climate that was more independent from the large-scale forcing and thus was more sensitive to
517 changes in the SST over the coupling domain. The coupled model thereby appeared to be a better model because of the
518 moderation of the ocean/seas on the atmosphere circulation. A detailed investigation of the effect of each difference
519 between the two CCLM versions is beyond the scope of this study and is a subject for future work. Second, the coupling
520 domain of COSTRICE over the North Sea extended towards the North Atlantic Ocean compared to RCA4-NEMO.
521 Previous studies have noted the importance of the North Atlantic for the weather over Europe, particularly with respect
522 to the NAO (Hurrell 1995, 1996; Greatbatch 2000). Folland et al. (2009) indicated that rainfall over northern European
523 and western Central Europe was significantly negatively correlated with the summer NAO index. Therefore, changes in
524 the SST and turbulent fluxes over the extended region of the coupling domain may have influenced the wind flow and
525 the moisture advection from the North Atlantic Ocean as it passed from the North Sea to Central Europe because of this
526 coupling. Under Northerly Circulation Type conditions, the northerly wind flow that prevailed over the North Atlantic

Ocean and Central Europe was strengthened; therefore, the large-scale moisture convergence over Central Europe was intensified in the coupled simulation. Consequently, the extreme summer precipitation was better reproduced by the COSTRICE model than the atmosphere-only CCLM model. Therefore, we configured RCA4-NEMO with the larger coupling domain that was used by COSTRICE to investigate whether this larger coupling domain could improve the precipitation that was simulated for Central Europe by RCA4.

However, both the large-scale moisture convergence from the North Sea and North Atlantic Ocean and that from other surrounding oceans, for instance, the Mediterranean Sea in southern Europe, play an important role in generating summer extreme precipitation over Central Europe. Several studies have noted the importance of the so-called 'Vb' cyclone track (van Bebber 1891) for heavy precipitation events over Central Europe (e.g., Muskulus and Jacob 2005), for which the Mediterranean Sea appears to be an important moisture source. This conclusion was true for the Elbe flood, although some disagreement exists regarding the overall contribution of the associated moisture flow. Sodemann et al. (2009) identified the North Atlantic Ocean as the most important moisture source. However, other studies (e.g., Stohl and James 2004; James et al. 2004) showed that the Mediterranean Sea more strongly contributed to this event than moisture from the North Atlantic Ocean. Ho-Hagemann et al. (2015) noted that large-scale moisture convergence that originated from both the North Atlantic Ocean and the Mediterranean Sea contributed to the heavy rainfall during phase 2 of the Oder flood event, which had a similar synoptic 'Vb' track as the Elbe flood. Therefore, atmosphere-ocean coupling over the Mediterranean Sea was planned for inclusion in the coupled CCLM systems to further reduce the dry bias in the simulated summer precipitation over Central Europe.

An issue that one should keep in mind while conducting air-sea coupling for any RCM is the potential inconsistency of SST and energy fluxes that cross the coupled domain to the uncoupled domain if a relaxation technique is not applied. For example, SSTs in TRIMNP were calculated based on fluxes from CCLM over the entire TRIMNP domain, which covered the North Atlantic until islands to the northwest and the Bay of Biscay to the southwest, the North Sea and the Baltic Sea. However, TRIMNP sent the SST to the CCLM only over the Baltic Sea, the eastern part of the North Sea, and a part of the North Atlantic Ocean along the Norwegian coast. The SST for CCLM over the remaining areas of the TRIMNP domain to the western boundary and over the area outside the TRIMNP domain was obtained from the ERA-Interim reanalysis data. Hence, SSTs in TRIMNP over the coupled area and uncoupled area may have contained a gradient because of the difference in fluxes from CCLM, which were calculated based on different SSTs. This SST gradient also caused an inconsistency when passed into CCLM. In fact, this second inconsistency exists in many current regional coupled atmosphere-ocean system models, such as COSTRICE and RCA4_NEMO-Nordic. This gradient is certainly not physical and thus should be "smoothed" using the relaxation technique, which is often applied to the sponge zone between RCM and the lateral boundary forcing. However, applying this technique to the boundary between coupled and uncoupled areas seems to be more difficult because this boundary often has a "zigzag" shape – a consequence of an interpolation of the ocean model domain (on another grid projection) to the (rotated) grid of the atmospheric model. Until now, this technique has not been implemented in any coupled model and the inconsistency remains unsolved.

An additional issue that should be considered in future studies is the resolution of atmospheric models. Although CCLM 5.0 in this study provided similar results for resolutions of 0.44° and 0.22°, the analysed precipitation was the average amount over Central Europe, where the distinct orography was less important. Using a higher resolution in the CCLM is strongly recommended to improve the simulations of extreme precipitation events over Europe. We expect that the effects of coupling for extreme event simulations may be different if a higher resolution (e.g., 0.11° or higher) is used in the atmospheric model; therefore, this recommendation also applies for future COSTRICE simulations. Other approaches for extreme precipitation analysis, such as considering the return periods of extreme events or using very-

high-resolution observation data (e.g., REGNI, DWD, over Germany), should be applied in future studies for such high-resolution simulations.

This study showed that the effect of coupling strongly depends on the considered timescales, the coupled system and the system configuration. The CCLM 4.8 simulations indicated that coupling over the North Sea and the Baltic Sea improved the simulation of summer heavy precipitation over Central Europe. The precipitation difference between the uncoupled and coupled simulations of RCA4 and CCLM 5.0 over Central Europe was, however, not very large, which may have been related to the lower sensitivity of the atmospheric model to changes in the SSTs because the atmospheric-only models were relatively stable. On the one hand, CCLM 5.0 was not sensitive to the initial conditions of the soil depth and several physical parameters at resolutions of 0.44° and 0.22°. On the other hand, CCLM 5.0 and RCA4 already exhibited rather good performance in simulating the large-scale circulation and summer precipitation over Central Europe, so not much room for improvement existed because of the use of coupled models. In addition, the smaller coupling domain over the North Sea in RCA4-NEMO than that of COSTRICE could be another reason for the small difference between the uncoupled and coupled simulations of RCA4. An ensemble of all the CCLM 4.8, CCLM 5.0 and RCA4 experiments showed that the coupled models statistically had equal skill as the uncoupled models in general and better performance in reproducing extreme events in particular. This result suggests that coupled models can be an effective tool for future projections. Analyses should be conducted for several RCMs (e.g., the CCLM and RCA4) that use the same resolution, coupling domains, SST forcings, and lateral boundary conditions to obtain more robust conclusions. Subsequently, the coupling area may be varied to identify the optimal domain for climate simulations over Europe. Additionally, investigating the effect of coupling when the atmospheric and ocean forcings for RCMs are not taken from reanalysis data but from global climate model simulations should prove insightful.

Acknowledgements

This study was supported by funding from the German project REKLIM. The research that was presented in this study is a part of the Baltic Earth Programme (Earth System Science for the Baltic Sea Region; see www.baltic-earth.eu), the Swedish Research Council for Environment, Agricultural Sciences and Spatial Planning (FORMAS) within the project "Impact of changing climate on circulation and biogeochemical cycles of the integrated North Sea and Baltic Sea system" (Grant no. 214-2010-1575) and Stockholm University's Strategic Marine Environmental Research Funds Baltic Ecosystem Adaptive Management (BEAM). Matthias Zahn was supported through the Cluster of Excellence ''CliSAP'' (EXC177), Universität Hamburg, which was funded through the German Science Foundation (DFG). The German Climate Computing Center (DKRZ) provided the computer hardware for the Limited Area Modelling simulations in the project "Regional Atmospheric Modelling". We acknowledge the E-OBS dataset from the EU-FP6 project ENSEMBLES (http://ensembles-eu.metoffice.com) and the data that were provided by the ECA&D project (http://www.ecad.eu). We appreciate the use of the ERA-Interim reanalysis product that was provided by the European Centre for Medium-Range Weather Forecasts (ECMWF). We acknowledge the NOAA High Resolution SST data that were provided by the NOAA/OAR/ESRL PSD, Boulder, Colorado, USA, from their website at http://www.esrl.noaa.gov/psd/. We express our thanks to Peter Hoffmann (Potsdam Institute for Climate Impact Research - PIK) for introducing and providing the weather type data from the German Weather Service (DWD).

Appendix A: Differences in the (a) MSLP (Pa), (b) T_2M (K), (c) T_2M-T_S (K; atm-ocn), (d) moisture convergence (mm/day), (e) sensible heat flux (W/m2) and (f) latent heat flux (W/m2) between the CPL_HZG and UNCPL_HZG averaged for very wet days in JJA from 1986–2009 for the Northerly Circulation Type.

List of Tables and Figures

Table 1. Experiment specifications as models, resolution, period and data used here.

Experiment	Model	Atm. Res. (degrees)	Ocean Res. (km)	SST over the North and Baltic Seas	Data available
UNCPL_HZG	CCLM 4.8	0.44		ERA-Int	1979-2009
CPL_HZG	COSTRICE 4.8	0.44	12.8	TRIMNP & CICE	1979-2009
UNCPL_SMHI	RCA4	0.22		ERA40	1961-2009
CPL_SMHI	RCA4-NEMO	0.22	3.7	NEMO-Nordic	1961-2009
UNCPL_HZG _rlwidth	CCLM 4.8 4 point sponge zone	0.44		ERA-Int	1979-2009
CPL_HZG _rlwidth	COSTRICE 4.8 4 point sponge zone	0.44	12.8	TRIMNP & CICE	1979-2009
UNCPL_HZGv5_044	CCLM 5.0	0.44		ERA-Int	1979-2009
CPL_HZGv5_044	COSTRICE 5.0	0.44	12.8	TRIMNP & CICE	1979-2009
UNCPL_HZGv5_044 _conf4.8	CCLM 5.0 Some parameters as 4.8	0.44		ERA-Int	1979-2009
CPL_HZGv5_044 _conf4.8	COSTRICE 5.0 Some parameters as 4.8	0.44	12.8	TRIMNP & CICE	1979-2009
UNCPL_HZGv5_022	CCLM 5.0	0.22		ERA-Int	1979-2009
CPL_HZGv5_022	COSTRICE 5.0	0.22	12.8	TRIMNP & CICE	1979-2009
UNCPL_HZGv5_022 _oldsoil	CCLM 5.0 old initial soil depth	0.22		ERA-Int	1979-2009
CPL_HZGv5_022 _oldsoil	COSTRICE 5.0 old initial soil depth	0.22	12.8	TRIMNP & CICE	1979-2009

Table 2. Different settings of CCLM 4.8 and CCLM 5.0.

Parameters	Definition	CCLM 4.8	CCLM 5.0
rlam_heat	Scaling factor for the thickness of the laminar boundary layer for heat	1.0	0.5249
tkhmin	Minimal diffusion coefficients for heat active in stable boundary layer conditions	0.1	0.35
tkmmin	Minimal diffusion coefficients for momentum active in stable boundary layer conditions	0.1	1.0
entr_sc	Entrainment rate for shallow convection	0.003	0.002
uc1	Variables for computing the rate of cloud cover in the unsaturated case	0.8	0.0626
v0snow	Factor in the terminal velocity for snow.	15	20
fac_rootdp2	Uniform multiplication factor for the prescribed root depth values	1	0.9
soilhyd	Uniform multiplication factor for hydraulic conductivity and diffusivity in the soil	1	1.62
itype_bbc_w	Option for choosing bottom boundary condition for vertical wind	-	1
itype_fast_wave	Parameter to select the treatment of fast waves	1	1 (modified)
itype_evsl	Parameter to select the type of parameterization for evaporation of bare soil	2 (BATS)	3 (ISBA)
itype_root	Parameter to select the type of root distribution	1	2 (Exponential)
itype_heatcond	Parameter to select the type of soil heat conductivity	1	2
limpltkediff	Switch to include horizontal turbulent diffusion if .TRUE.	-	.FALSE.

Table 3. Means (mm/day) and the 90th and 95th percentiles (i.e., PC90 and PC95; mm/day) of the daily summer precipitation averaged over Central Europe for the period from 1986–2009 for the E-OBS data and the experiments.

Data	Mean	PC90	PC95
E-OBS	2.54	6.14	7.90
UNCPL_HZG	1.68	4.81	6.67
CPL_HZG	1.75	5.03	6.78
coastDat2	1.73	4.55	5.97
UNCPL_SMHI	2.83	6.80	8.55
CPL_SMHI	2.80	6.68	8.20

Table 4. Statistical scores (ME, MAE, RMSE, Correlation coefficient Corr.) of the ensemble mean of 6 uncoupled (UNCPL) and 6 coupled (CPL) experiments of CCLM against the E-OBS data of the daily summer precipitation averaged over Central Europe for very wet days of the Northerly Circulation Type in JJA 1986–2009. In "()" is values of the ensemble including the SMHI's simulations.

E-OBS (mean = 8.06)	UNCPL	CPL
Mean	5.56 (5.67)	5.79 (5.82)
ME	-2.50 (-2.39)	-2.27 (-2.24)
MAE	2.84 (2.77)	2.72 (2.69)
RMSE	3.63 (3.52)	3.41 (3.38)
Corr.	0.67 (0.67)	0.71 (0.70)

Fig. 1 Integration domain of the CCLM (whole domain), including the sponge zone (grey area), TRIMNP (dark-blue and light-blue), and CICE (light-blue). Central Europe is marked by the red box.

Fig. 2 Seasonal mean of the observation (the first column) and biases (four next columns) of experiments to the observation of (a) mean sea-level pressure against the ERA-Int data, (b) air temperature at a 2 m height against the E-OBS data, (c) sea surface temperature against the OISSTv2 data, and (d) precipitation against the E-OBS data averaged for summer (JJA) for the period 1986–2009. Grey colour denotes missing values.

Fig. 3 Daily precipitation (mm/day) of the E-OBS data and various experiments for six circulation types for very wet days. Data are averaged over Central Europe (see Fig. 1) for the summer months (JJA) from 1986–2009. Numbers in "[ ]" on the x-axis show the number of days that the circulation type was observed.

Fig. 4 Daily mean of the observation (the first column) and biases (four next columns) of experiments to the observation of (a) mean sea-level pressure against the ERA-Int data, (b) sea surface temperature against the OISSTv2 data, and (c) precipitation against the E-OBS data averaged for very wet days in JJA for 1986–2009 for the Northerly Circulation Type. Grey colour denotes missing values.

Fig. 5 Differences in the (a) daily mean SST (K), (b) wind speed (m/s), (c) precipitable water (mm/day) and (d) precipitation (mm/day) between the CPL_HZG and UNCPL_HZG averaged for very wet days in JJA for 1986–2009 for the Northerly Circulation Type.

Fig. 6 Differences in the (a) daily mean SST (K), (b) wind speed (m/s), (c) precipitable water (mm/day) and (d) precipitation (mm/day) between CPL_SMHI and UNCPL_SMHI, averaged for very wet days in JJA for 1986–2009 for the Northerly Circulation Type. Grey colour denotes missing values.

Fig. 7 Air-sea feedback and interaction diagram. For each arrow, the initial status indicates that the source quantity is increasing, and the sign (- or +) indicates the changing tendency of the target quantity. Colours denote the group of changes or states over sea (blue), land (brown) and the land-sea interactions (green).

Fig. 8 Daily precipitation differences (mm/day) between the coupled and uncoupled CCLM (top row) and RCA4 (bottom row) for summer (JJA) for the period 1986–2009. The left column shows the difference in heavy precipitation (exceeds the 90^{th} percentile). White colour denotes missing values. The right column shows only the differences that are significant at the 95% confidence level (tested with a 2-sided t-test). (a) For the entire time series; and (b) for the Northerly Circulation Type.

Fig. 9 Daily precipitation (mm/day) of the E-OBS data (light-blue bars), uncoupled (blue triangles) and coupled (red asterisks) simulations averaged for Central Europe for 98 very wet days of the Northerly Circulation Type in JJA 1986-2009. (a) UNCPL_HZG and CPL_HZG v4.8; (b) Ensemble of UNCPL_HZG and CPL_HZG v4.8; (c) UNCPL_SMHI and CPL_SMHI; (d) UNCPL_HZG and CPL_HZG v5.0 on 0.44^{o} grid; (e) UNCPL_HZG and CPL_HZG v5.0 on 0.22^{o} grid; (f) UNCPL_HZG and CPL_HZG ensemble mean.

Fig. 10 Daily precipitation bias (mm/day) of the ensemble of 7 uncoupled CCLMs (blue) and 7 coupled CCLMs (red) against the E-OBS data averaged for Central Europe for 98 very wet days of the Northerly Circulation Type in JJA 1986-2009. The shaded areas show ranges between minimum and maximum biases of the ensemble. The solid lines display the mean bias of the ensemble. (a) Including the SMHI's simulations; (b) Excluding the SMHI's simulations.

676 **References**

677 Aldrian E, Sein D, Jacob D, Dumenil Gates L, Podzun R (2005) Modeling Indonesian rainfall with a coupled regional
678 model. Clim Dyn 25:1–17

679 Anders I, Rockel B (2009) The influence of prescribed soil type distribution on the representation of present climate in
680 a regional model, Clim Dyn 33:177-186

681 Artale V, Calmanti S, Carillo A et al. (2009) An atmosphere-ocean regional climate model for the mediterranean area:
682 assessment of a present climate simulation. Clim Dyn 35:721–740

683 Balmaseda MA, Mogensen K, Weaver AT (2013) Evaluation of the ECMWF Ocean Reanalysis ORAS4. Q J R
684 Meteorol Soc. DOI:10.1002/qj.2063

685 Bender MA, Ginis I, Kurihara Y (1993) Numerical simulations of hurricane-ocean interaction with a high resolution
686 coupled model. J Geophys Res 98:23245-23263

687 Betts AK, Ball JH, Beljaars ACM, Miller MJ, Viterbo PA (1996) The land-surface atmosphere interaction: A review
688 based on observational and global modeling perspectives. J Geophys Res 101:7209-7225

689 Boberg F, Berg P, Thejll P, Gutowski W, Christensen J (2010) Improved confidence in climate change projections of
690 precipitation further evaluated using daily statistics from ENSEMBLES models. Clim Dyn 35(7–8):1509–1520.
691 doi:10.1007/s00382-009-0683-8

692 Casulli V, Cattani E (1994) Stability, Accuracy and Efdiciency of a Semi-Implicit Method for Three-Dimensional
693 Shallow Water Flow. Computers Math Applic 27:99–112

694 Casulli V, Stelling GS (1998) Numerical Simulation of 3D Quasi-Hydrostatic, Free-Surface Flows, J Hydr Engrg
695 124:678–686

696 Champeaux JL, Masson V, Chauvin F (2005) ECOCLIMAP: a global database of land surface parameters at 1 km
697 resolution. Met Apps 12:29-32. doi: 10.1017/S1350482705001519

698 Christensen J, Boberg F, Christensen O, Lucas-Picher P (2008) On the need for bias correction of regional climate
699 change projections of temperature and precipitation. Geophys Res Lett 35:L20709. doi:10.1029/2008GL0356

700 Dee DP, Uppala SM, Simmons AJ et al (2011) The ERA-interim reanalysis: Configuration and performance of the data
701 assimilation system. Q J R Meteor Soc 137:553-597. doi: 10.1002/qj.828

702 Dieterich C, Schimanke S, Wang S et al (2013) Evaluation of the SMHI coupled atmosphere-ice-ocean model RCA4-
703 NEMO. SMHI Report Oceanography 47, 80pp

704 Dirmeyer P, Koster R, Guo ZAD (2006) Do global models properly represent the feedback between land and
705 atmosphere? J Hydrometeor 7: 1177-1198

706 Doms GJF, Heise E, Herzog H-J et al (2011) A Description of the Nonhydrostatic Regional COSMO Model. Part II:
707 Physical Parameterization. Tech. Rep. Deutscher Wetterdienst, available at: http://www.cosmo-
708 model.org/content/model/documentation/core/cosmoPhysParamtr.pdf

709 Döscher R, Willén U, Jones C et al (2002) The development of the regional coupled ocean-atmosphere model RCAO.
710 Boreal Environ Res 7:183–192

711 Folland CK, Knight J, Linderholm HW et al (2009) The summer North Atlantic Oscillation: Past, present, and future. J
712 Clim 22(5):1082-1103. doi:10.1175/2008JCLI2459.1

713 Geyer B (2014) High-resolution atmospheric reconstruction for Europe 1948–2012: coastDat2. Earth Syst Sci Data
714 6:147-164. doi:10.5194/essd-6-147-2014

715 Gimeno L, Drumond A, Nieto R, Trigo RM, Stohl A (2010) On the origin of continental precipitation. Geophys Res
716 Lett 37:L13804

717 Giorgi F (2006) Regional climate modeling: Status and Perspectives. Journal de Physique IV (139):101-118

718 Giorgi F, Jones C, Asrar GR (2009) Addressing climate information needs at the regional level: the CORDEX
719 framework, WMO Bulletin (58): 175-183

720 Greatbatch RJ (2000) The North Atlantic Oscillation. Stochastic Environmental Research and Risk Assessment 14
721 (4+5):213-242

722 Gröger M, Dieterich C, Meier HEM, Schimanke S (2015) Thermal air-sea coupling in hindcast simulations for the
723 North Sea and Baltic Sea on the NW European shelf. Tellus A (67), 26911.
724 http://dx.doi.org/10.3402/tellusa.v67.26911

725 Gustafsson N, Nyberg L, Omstedt A (1998) Coupling of a High-Resolution Atmospheric Model and an Ocean Model

for the Baltic Sea. Monthly Weather Rev 126:2822-2846

Hagedorn R, Lehmann A, Jacob D (2000) A coupled high resolution atmosphere-ocean model for the BALTEX region. Meteorologische Zeitschrift 9:7-20

Hagemann S, Botzet M, Machenhauer B (2001) The summer drying problem over south-eastern Europe: Sensitivity of the limited area model HIRHAM4 to improvements in physical parameterization and resolution. Physics and Chemistry of the Earth, Part B 26:391-396

Hagemann S, Machenhauer B, Jones R et al (2004) Evaluation of water and energy budgets in regional climate models applied over Europe. Clim Dyn 23:547-567. doi: 10.1007/s00382-004-0444-7

Harris I, Jones PD, Osborn TJ, Lister DH (2013) Updated high-resolution grids of monthly climatic observations - the CRU TS3.10 dataset. International Journal of Climatology. doi:10.1002/joc.3711

Haylock MR, Hofstra N, Klein Tank AMG et al (2008) A European daily high-resolution gridded data set of surface temperature and precipitation for 1950-2006. Journal of Geophysical Research 113: D20119. doi:10.1029/2008JD010201

Hewitt HT, Copsey D, Culverwell ID et al (2011) Design and implementation of the infrastructure of HadGEM3: the next-generation Met Office climate modelling system, Geosci. Model Dev. (4): 223-253, doi:10.5194/gmd-4-223-2011

Ho-Hagemann HTM, Rockel B, Kapitza H, Geyer B, Meyer E (2013) COSTRICE - an atmosphere - ocean - sea ice model coupled system using OASIS3. HZG Report 2013-5, 26pp

Ho-Hagemann HTM, Hagemann S, Rockel B (2015) On the role of soil moisture in the generation of heavy rainfall during the Oder flood event in July 1997. Tellus A (67), 28661. doi:10.3402/tellusa.v67.28661

Hunke EC, Lipscomb WH, Turner AK, Jeffery N, Elliott S (2013) CICE: The Los Alamos Sea Ice Model Documentation and Software User's Manual Version 5.0 LA-CC-06–012. Los Alamos National Laboratory, USA

Hurrell JW (1995) Decadal trends in the North Atlantic Oscillation: Regional temperatures and precipitation. Science 269:676-679

Hurrell JW (1996) Influence of variations in extratropical wintertime teleconnections on Northern Hemisphere temperature. Geophys Res Lett 23:665-668

James PM (2006) An assessment of European synoptic variability in Hadley Centre Global Environmental models based on an objective classification of weather regimes, Clim Dyn 27:215–231. doi:10.1007/s00382-006-0133-9

James PM (2007) An objective classification method for Hess and Brezowsky Grosswetterlagen over Europe. Theoretical and Applied Climatology 88:17-42

James P, Stohl A, Spichtinger N, Eckhardt S, Forster C (2004) Climatological aspects of the extreme European rainfall of August 2002 and a trajectory method for estimating the associated evaporative source regions. Nat. Hazards Earth Syst Sci 4:733-746. doi:10.5194/nhess-4-733-2004

Kalnay E, Kanamitsu M, Kistler R et al (1996) The NCEP/NCAR 40-Year Reanalysis Project. Bull Amer Meteor Soc 77:437–471

Kistler R, Kalnay E, Collins W et al (2001) The NCEP-NCAR 50-Year Reanalysis: Monthly Means CD-ROM and Documentation. Bull Amer Meteor Soc 82:247–268

Koster RD, Dirmeyer PA, Guo Z et al (2004) Regions of strong coupling between soil moisture and precipitation. Science 305 (5687): 1138–1140

Kotlarski S, Keuler K, Christensen OB et al (2014) Regional climate modelling on European scales: A joint standard evaluation of the EURO-CORDEX RCM ensemble. Geoscientific Model Development 7:1297-1333

Kupiainen M, Jansson C, Samuelsson P et al (2014) Rossby Centre regional atmospheric model, RCA4. Rossby Center News Letter. Online at: http://www.smhi.se/en/Research/Research-departments/climate-research-rossby-centre2-552/1.16562

Larsen MAD, Christensen JH, Drews M, Butts MB, Refsgaard JC (2016) Local control on precipitation in a fully coupled climate-hydrology model. Sci Rep 6, 22927; doi: 10.1038/srep22927

Li LZX (2006) Atmospheric GCM response to an idealized anomaly of the Mediterranean sea surface temperature, Clim Dyn 27:543–552

Machenhauer B, Windelband M, Botzet M et al (1998) Validation and analysis of regional present-day climate and climate simulations over Europe. MPI Report. Max-Planck-Inst., Hamburg, Germany

Madec G (2008) NEMO ocean engine. Tech Rep 27. Note du Pole de modélisation, Institut Pierre-Simon Laplace 1280 (IPSL), France

778 Maykut GA, Untersteiner N (1971) Some results from a time dependent thermodynamic model of sea ice. J. Geophys.
779 Res. (76):1550–1575

780 Meehl GA (1994) Coupled land-ocean-atmosphere processes and south Asian monsoon variability. Science 266:263-
781 267, doi:10.1126/science.266.5183.263.

782 Meier HEM, Höglund A, Döscher R, Andersson H, Löptien U, Kjellström E (2011) Quality assessment of atmospheric
783 surface fields over the Baltic Sea of an ensemble of regional climate model simulations with respect to ocean
784 dynamics. Oceanologia 53:193-227

785 Muskulus M, Jacob D (2005) Tracking cyclones in regional model data: The future of Mediterranean storms. Adv
786 Geosci 2:13-19. doi:10.5194/adgeo-2-13-2005

787 Nabat P, Somot S, Mallet M et al (2015) Direct and semi-direct aerosol radiative effect on the Mediterranean climate
788 variability using a coupled regional climate system model. Clim Dyn 44:1127. doi:10.1007/s00382-014-2205-6

789 Pham VT, Brauch J, Dieterich C, Frueh B, Ahrens B (2014) New coupled atmosphere-ocean-ice system COSMO-
790 CLM/NEMO: assessing air temperature sensitivity over the North and Baltic Seas. Oceanologia 56 (2).
791 doi:10.5697/oc.56-2.167

792 Ratnam JV, Giorgi F, Kaginalkar A, Cozzini S (2009) Simulation of the Indian monsoon using the RegCM3-ROMS
793 regional coupled model. Clim Dyn 33:119-139.

794 Räisänen J, Hansson U, Ullerstig U et al (2004) European climate in the late 21st century: regional simulations with two
795 driving global models and two forcing scenarios. Clim Dyn 22:13-31

796 Reynolds RW, Smith TM, Liu C et al (2007) Daily High-Resolution-Blended Analyses for Sea Surface Temperature. J
797 Clim 20:5473-5496

798 Rockel B, Will A, Hense A (ed) (2008) Special issue Regional climate modelling with COSMO-CLM (CCLM).
799 Meteorologische Zeitschrift 17(4):347-348

800 Rummukainen M, Räisänen J, Bringfelt B et al (2001) A regional climate model for northern Europe: model description
801 and results from the downscaling of two GCM control simulations. Clim Dyn 17:339-359

802 Samuelsson P et al (2011) The Rossby Centre Regional Climate model RCA3: model description and performance.
803 Tellus A (63), 423

804 Schrodin R, Heise E (2001) The multi-layer-version of the DWD soil model TERRA/LM, Consortium for Small-Scale
805 Modelling (COSMO). Tech. Rep. (2):16 pp

806 Schrum C, Huebner U, Jacob D, Podzum R (2003) A coupled atmosphere/ice/ocean model for the North Sea and the
807 Baltic Sea. Clim Dyn 21:131–151

808 Schrum C (2016): Regional Climate modeling and air-sea coupling. Climate Science, Oxford Research Encyclopdias,
809 DOI: 10.1093/acrefore/9780190228620.013.3

810 Seneviratne SI, Pal JS, Eltahir EAB, Schär C (2002) Summer dryness in a warmer climate: A process study with a
811 regional climate model. Clim Dyn 20:69- 85

812 Seneviratne SI, Lüthi D, Litschi M, Schär C (2006) Land–atmosphere coupling and climate change in Europe. Nature
813 443(7108):205–209

814 Seneviratne SI, Stöckli R (2008) The role of land-atmosphere interactions for climate variability in Europe. In: Climate
815 Variability and Extremes during the Past 100 years, Brönnimann et al. (eds.), Adv Global Change Res 33, Springer
816 Verlag (Book chapter)

817 Seneviratne SI, Corti T, Davin E, Hirschi M, Jaeger EB et al (2010) Investigating soil moisture-climate interactions in a
818 changing climate: a review. Earth Sci Rev 99:125-161

819 Shrestha P, Sulis M, Masbou M, Kollet S, Simmer C (2014) A scale-consistent terrestrial systems modeling
820 platform based on COSMO, CLM, and Parflow. Mon Weather Rev 142:3466–3483

821 Sodemann H, Wernli H, Schwierz C (2009) Sources of water vapour contributing to the Elbe flood in August 2002 – A
822 tagging study in a mesoscale model. Q J Roy Meteorol Soc 135:205–223. doi:10.1002/qj.374

823 Stohl A, James P (2004) A Lagrangian analysis of the atmospheric branch of the global water cycle, Part I: Method
824 description, validation, and demonstration for the August 2002 flooding in Central Europe. J Hydrometeorol
825 5:656–678. doi:10.1175/1525-7541(2004)005<0656:ALAOTA>2.0.CO;2

826 Somot A, Sevault F, Deque M, Crepon M (2008) 21st century climate change scenario for the Mediterranean using a
827 coupled Atmosphere-Ocean Regional Climate Model. Global and Planetary Change, Elsevier, 63 (2-3):112-126

828 Tian T, Boberg F, Bøssing Christenssen O et al (2013) Resolved complex coastlines and land_sea contrasts in a high-
829 resolution regional climate model: a comparative study using prescribed and modelled SSTs. Tellus A (65), 19951.

http://dx.doi.org/10.3402/tellusa.v65i0.19951

Tiedtke M (1989) A comprehensive mass flux scheme for cumulus parameterization in large-scale models. Monthly weather review (117):1779-1799

Turner AK, Hunke EC, Bitz CM (2013) Two modes of sea-ice gravity drainage: a parameterization for large-scale modeling. J. Geophys. Res. (118):2279–2294, doi:10.1002/jgrc.20171

Untersteiner N (1964) Calculations of temperature regime and heat budget of sea ice in the Central Arctic. J. Geophys. Res. (69):4755–4766

Uppala SM, Kallberg PW, Simmons AJ et al (2005) The ERA-40 re-analysis. Quart J R Meteor Soc 131:2961–3012. doi:10.1256/qJ04.176

U.S. Geological Survey (2004) Global digital elevation model (gtopo30). Technical Report. EROS Data Center Distributed Active Archive Center (EDC DAAC)

Valcke S, Craig T, Coquart L (2013) OASIS3-MCT User Guide, OASIS3-MCT 2.0. Technical Report, TR/CMGC/13/17, CERFACS/CNRS SUC URA No 1875, Toulouse, France

van Bebber WJ (1891) Die Zugstrassen der barometrischen Minima nach den Bahnenkarten der Deutschen Seewarte fur den Zeitraum von 1870 – 1890. Meteorologische Zeitschrift 8:361-366

van der Ent RJ, Savenije HHG, Schaefli B, Steele-Dunne SC (2010) Origin and fate of atmospheric moisture over continents. Water Resources Research 46, W09525. doi:10.1029/2010WR009127

Vancoppenolle M, Fichefet T, Goosse H, Bouillon S, Madec G, Maqueda M (2009) Simulating the mass balance and salinity af arctic and antarctic sea ice. Ocean Modelling 27:33–53

Vidale PL, Lüthi D, Frei C, Seneviratne SI, Schär C (2003) Predictability and uncertainty in a regional climate model, J Geophys Res 108 (D18), 4586. doi:10.1029/2002JD002810

von Storch H, Langenberg H, Feser F (2000) A Spectral Nudging Technique for Dynamical Downscaling Purposes. Mon Wea Rev 128:3664–3673

Wang S, Dieterich C, Döscher R , Höglund A, Hordoir R, Meier HEM, Samuelsson P, Schimanke S (2015) Development and evaluation of a new regional coupled atmosphere-ocean model RCA4-NEMO and application for future scenario experiments. Tellus A (67), 24284

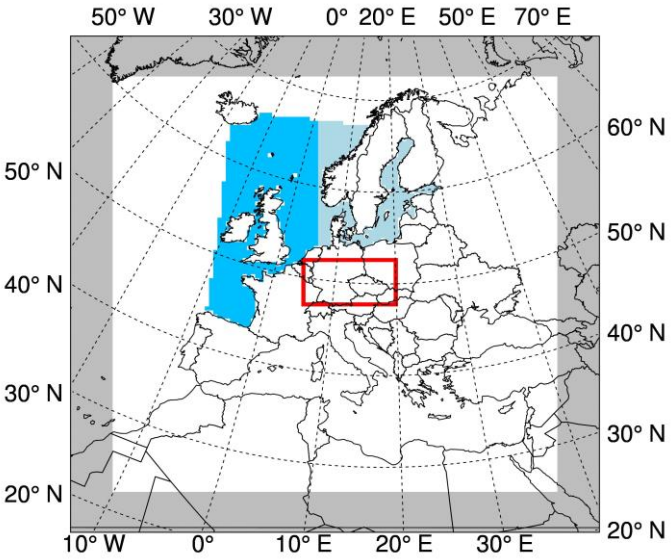

857

858 **Fig.1** Integration domain of the CCLM (whole domain), including the sponge zone (grey area), TRIMNP (dark-blue and
859 light-blue), and CICE (light-blue). Central Europe is marked by the red box.

860

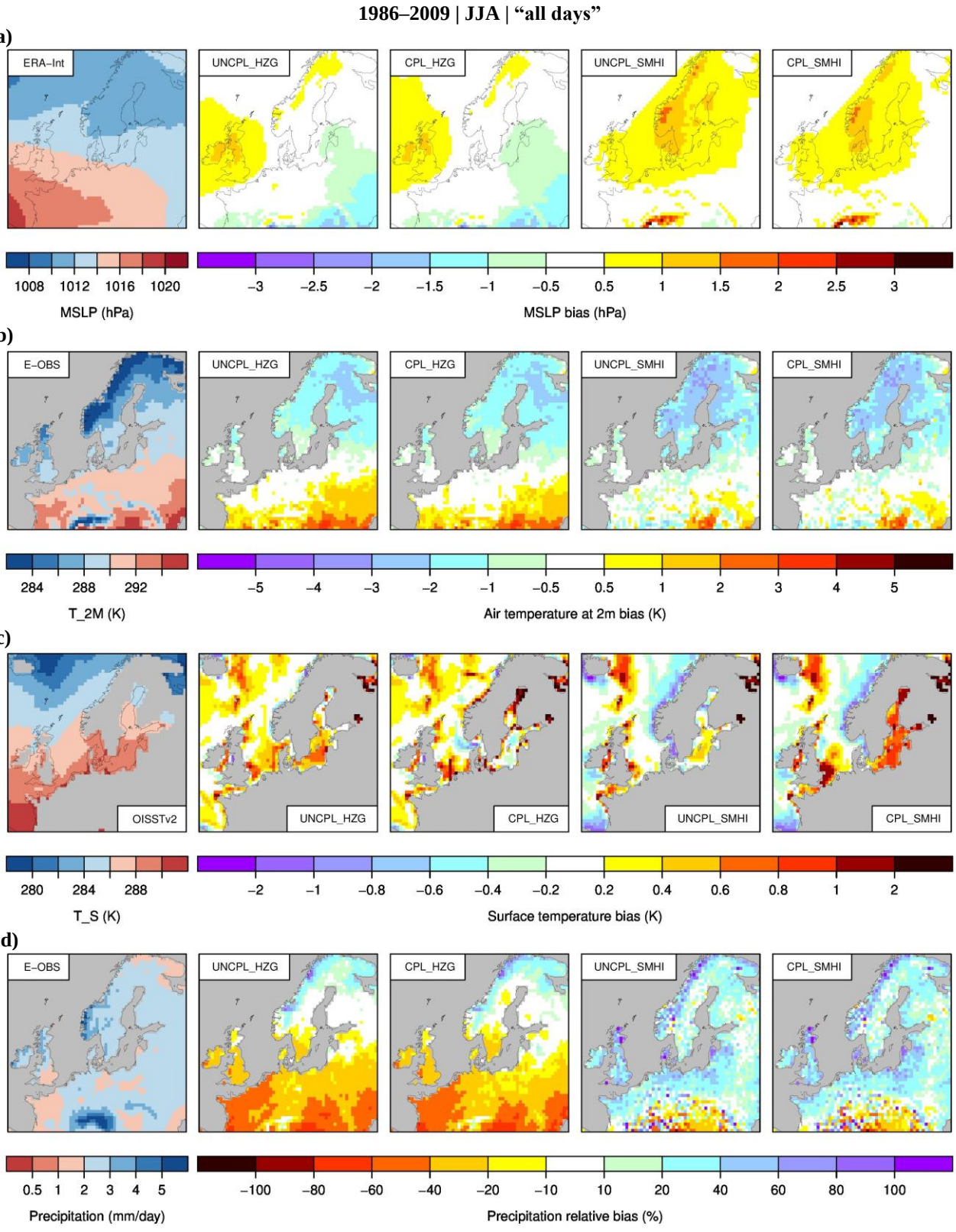

Fig.2 Seasonal mean of the observation (the first column) and biases (four next columns) of experiments to the observation of (a) mean sea-level pressure against the ERA-Int data, (b) air temperature at a 2 m height against the E-OBS data, (c) sea surface temperature against the OISSTv2 data, and (d) precipitation against the E-OBS data averaged for summer (JJA) for the period 1986–2009. Grey colour denotes missing values.

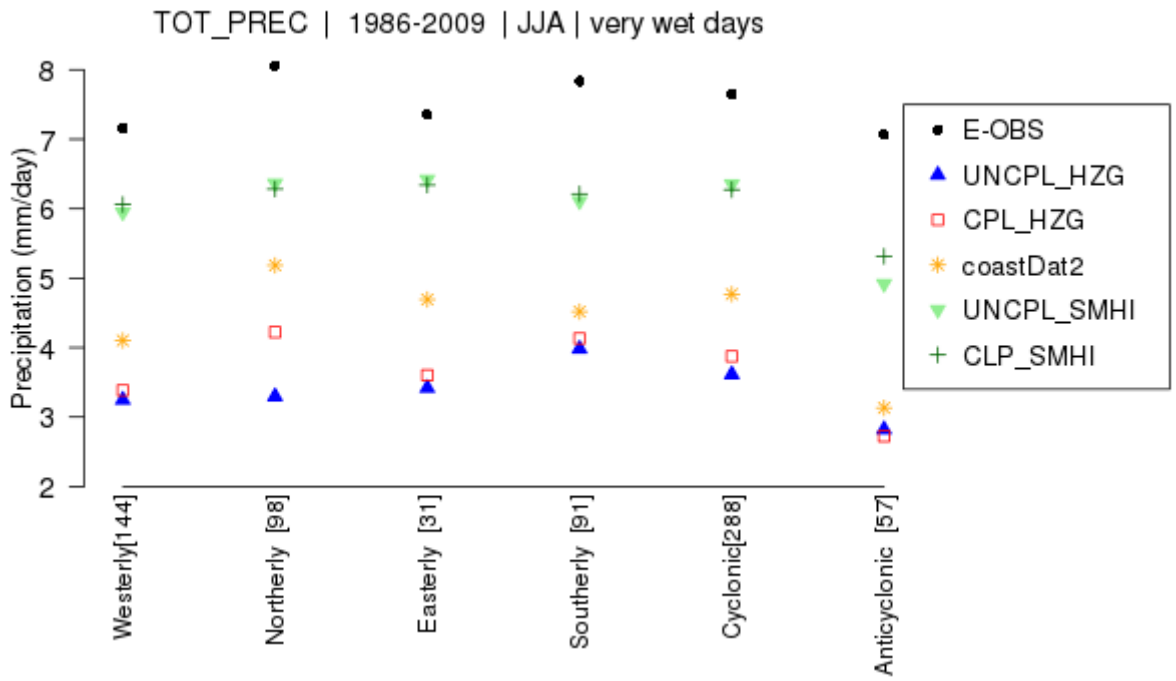

Fig.3 Daily precipitation (mm/day) of the E-OBS data and various experiments for six circulation types for very wet days. Data are averaged over Central Europe (see Fig. 1) for the summer months (JJA) from 1986–2009. Numbers in "[ ]" on the x-axis show the number of days that the circulation type was observed.

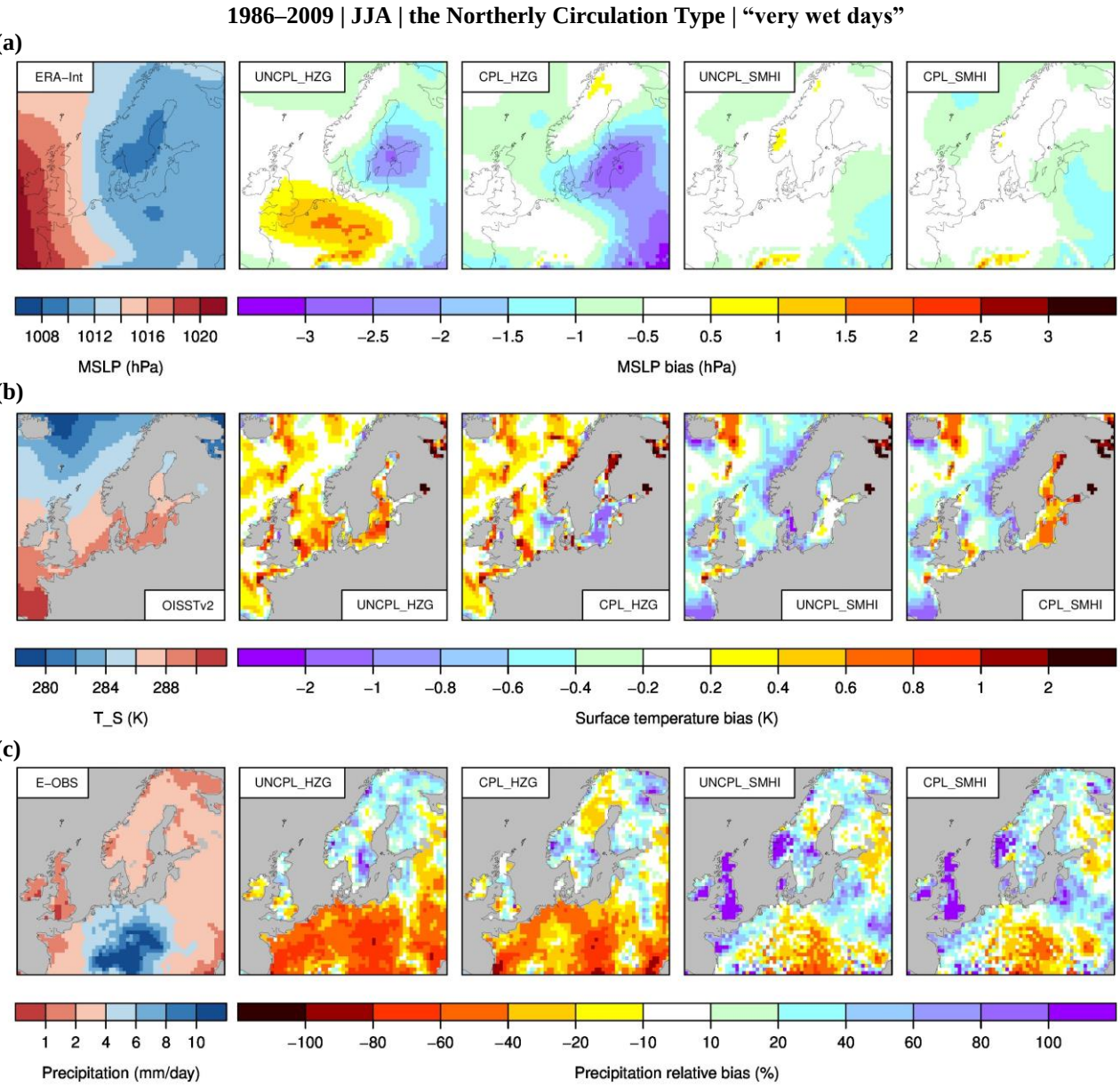

Fig.4 Daily mean of the observation (the first column) and biases (four next columns) of experiments to the observation of (a) mean sea-level pressure against the ERA-Int data, (b) sea surface temperature against the OISSTv2 data, and (c) precipitation against the E-OBS data averaged for very wet days in JJA for 1986–2009 for the Northerly Circulation Type. Grey colour denotes missing values.

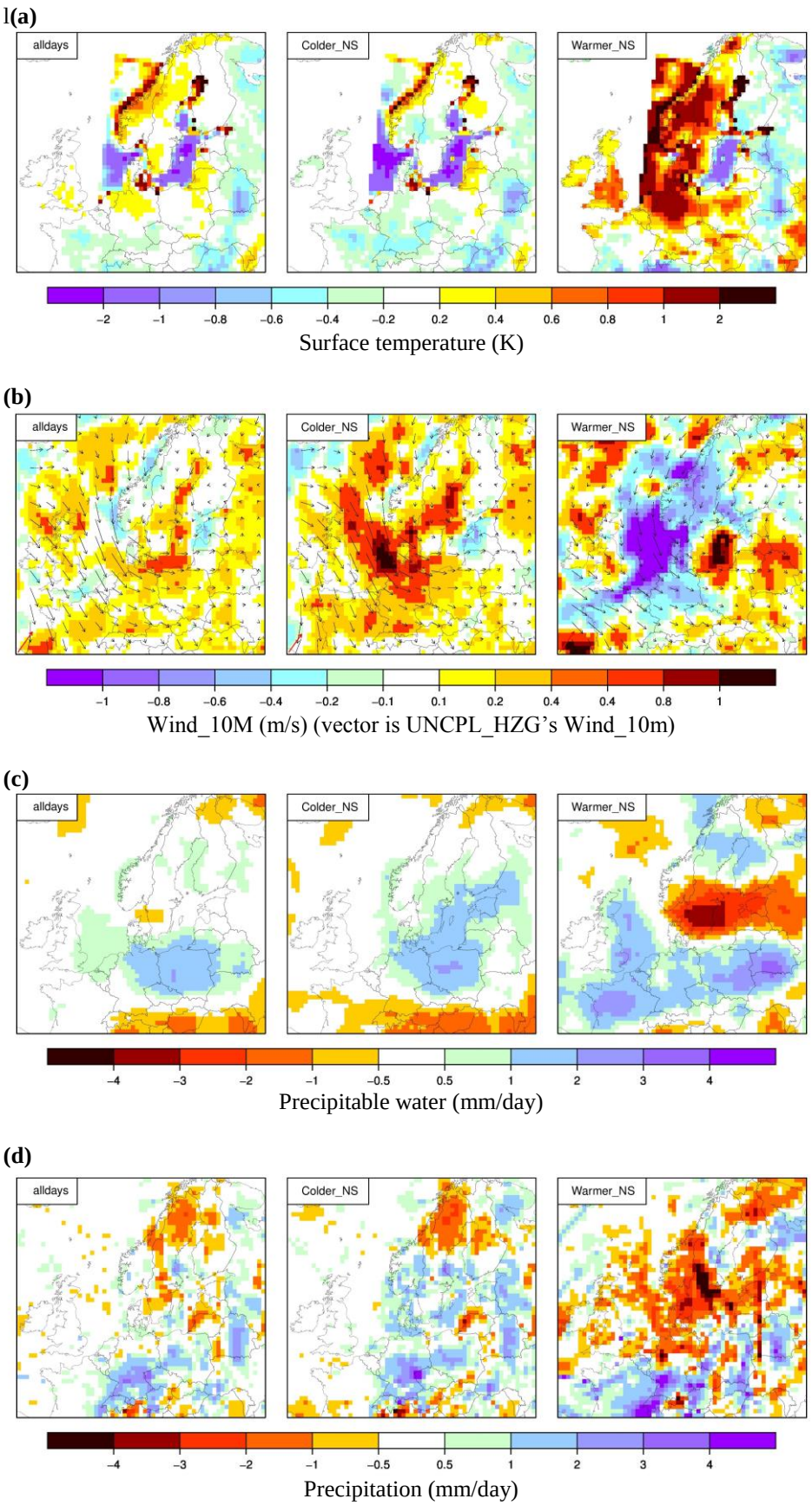

Fig.5 Differences in the (a) daily mean SST (K), (b) wind speed (m/s), (c) precipitable water (mm/day) and (d) precipitation (mm/day) between the CPL_HZG and UNCPL_HZG averaged for very wet days in JJA for 1986–2009 for the Northerly Circulation Type.

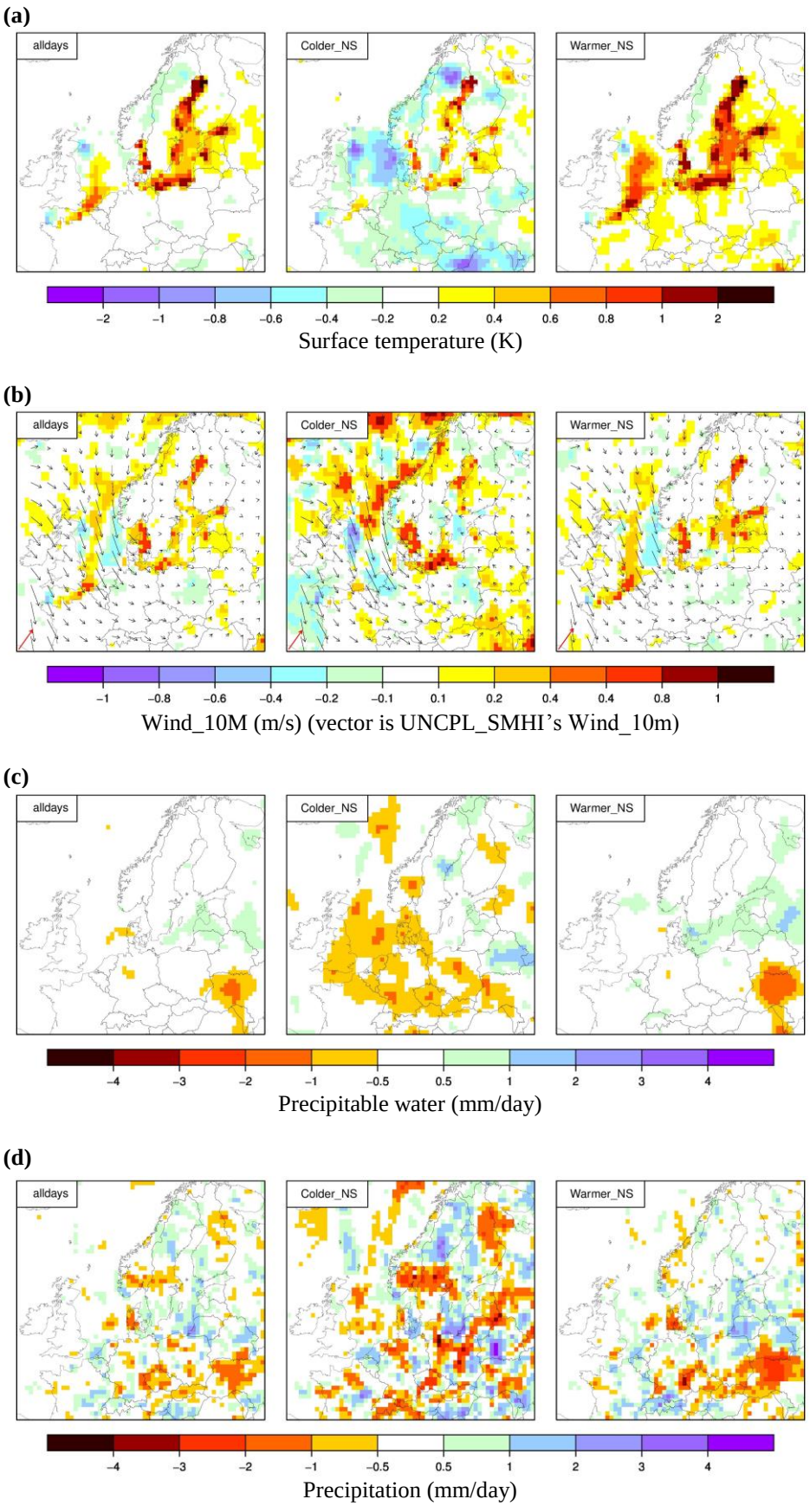

Fig.6 Differences in the (a) daily mean SST (K), (b) wind speed (m/s), (c) precipitable water (mm/day) and (d) precipitation (mm/day) between CPL_SMHI and UNCPL_SMHI, averaged for very wet days in JJA for 1986–2009 for the Northerly Circulation Type. Grey colour denotes missing values.

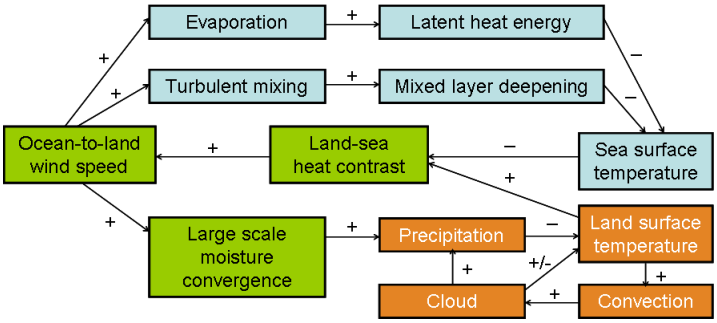

Fig.7 Air-sea feedback and interaction diagram. For each arrow, the initial status indicates that the source quantity is increasing, and the sign (– or +) indicates the changing tendency of the target quantity. Colours denote the group of changes or states over sea (blue), land (brown) and the land-sea interactions (green).

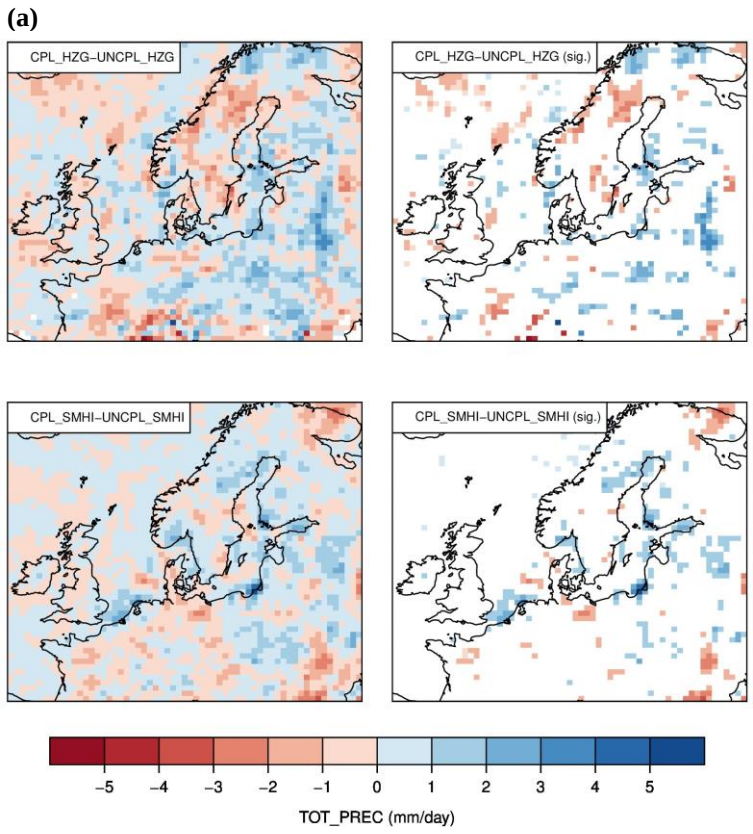

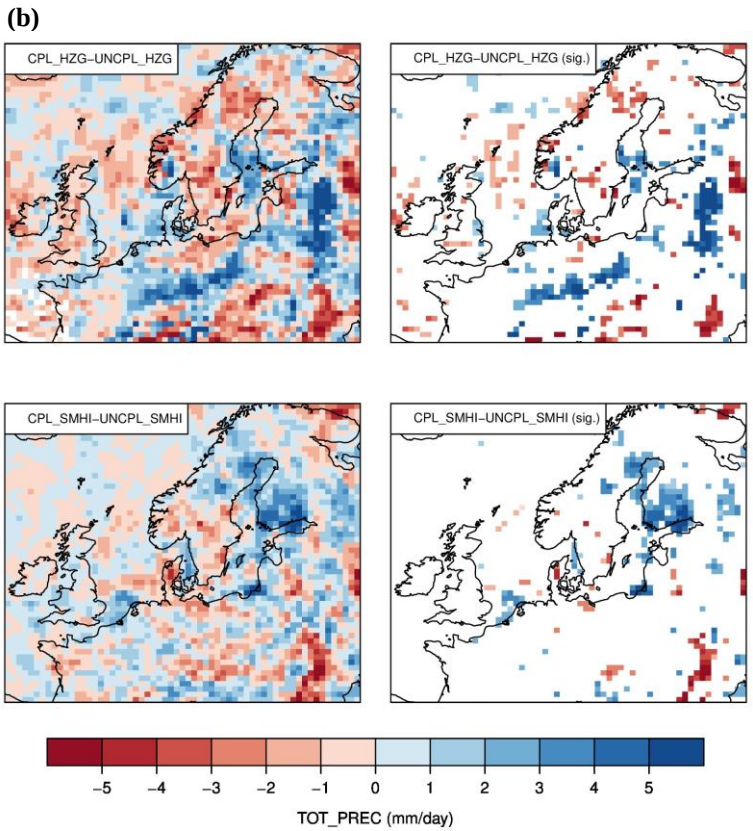

Fig.8 Daily precipitation differences (mm/day) between the coupled and uncoupled CCLM (top row) and RCA4 (bottom row) for summer (JJA) for the period 1986–2009. The left column shows the difference in heavy precipitation (exceeds the 90th percentile). White colour denotes missing values. The right column shows only the differences that are significant at the 95% confidence level (tested with a 2-sided t-test). (a) For the entire time series; and (b) for the Northerly Circulation Type.

(a) UNCPL_HZG and CPL_HZG (v4.8, res. 0.44º)

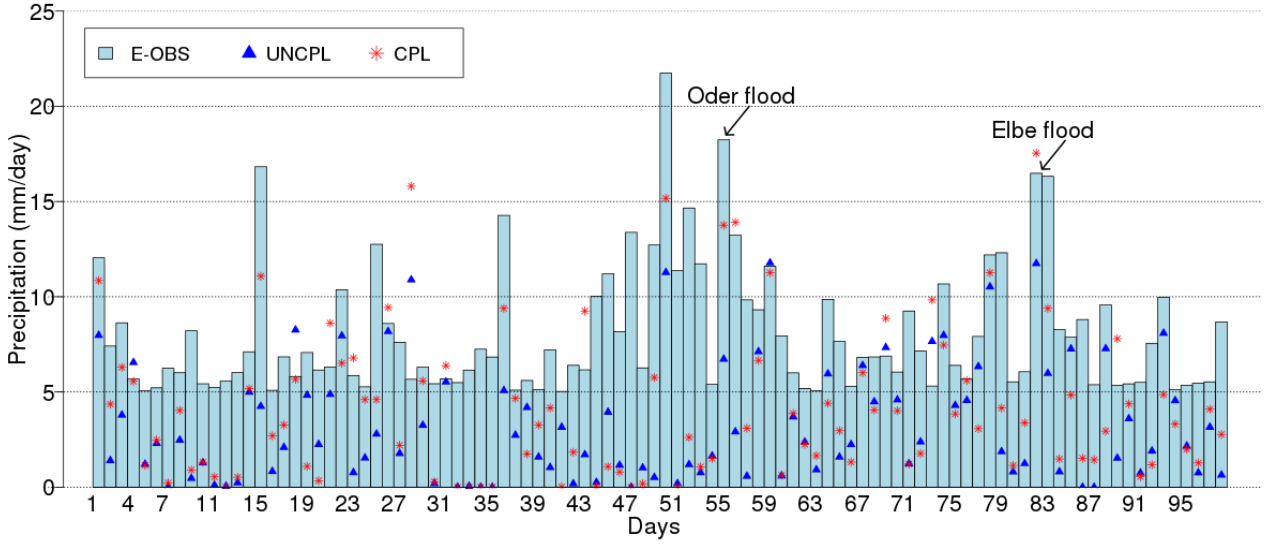

(b) Ensemble of UNCPL_HZG and CPL_HZG (v4.8, res. 0.44º)

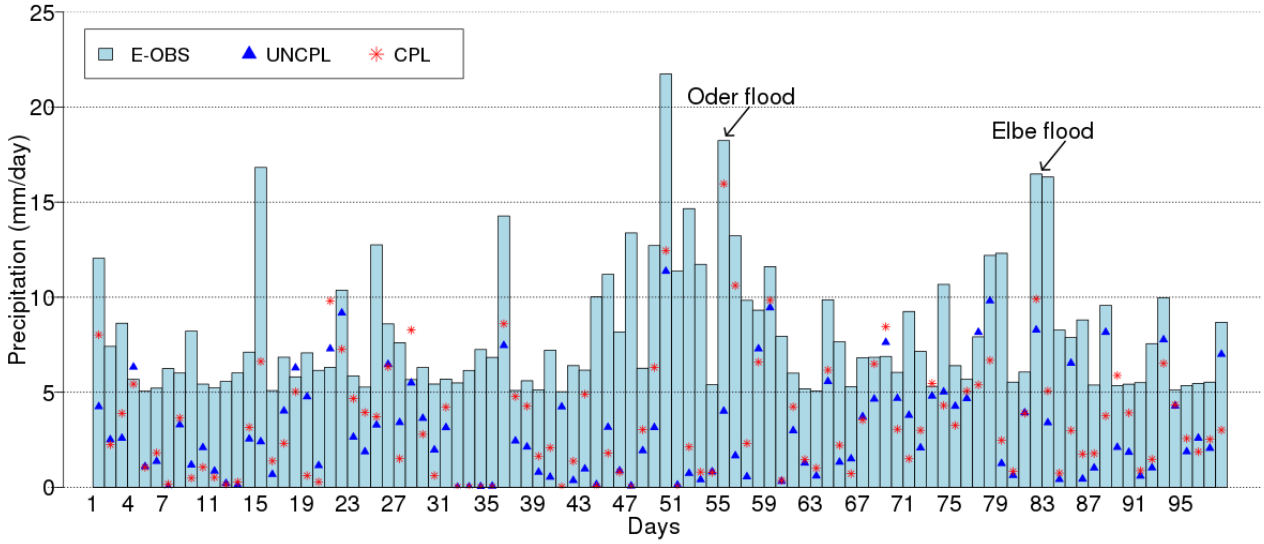

(c) UNCPL_SMHI and CPL_SMHI

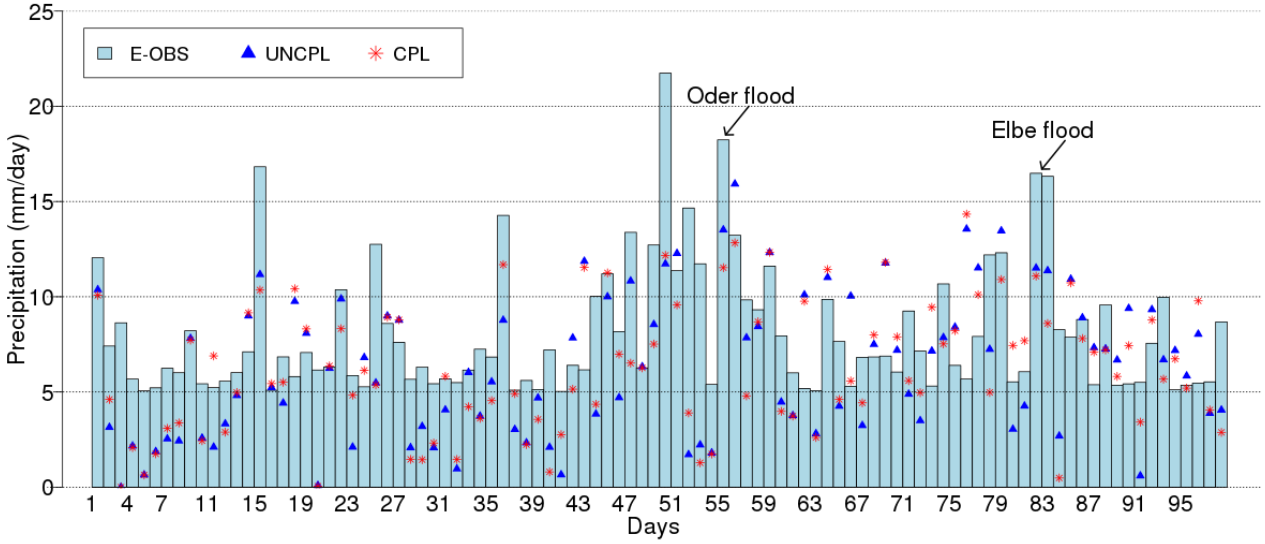

(d) UNCPL_HZG and CPL_HZG (v5.0, res. 0.44º)

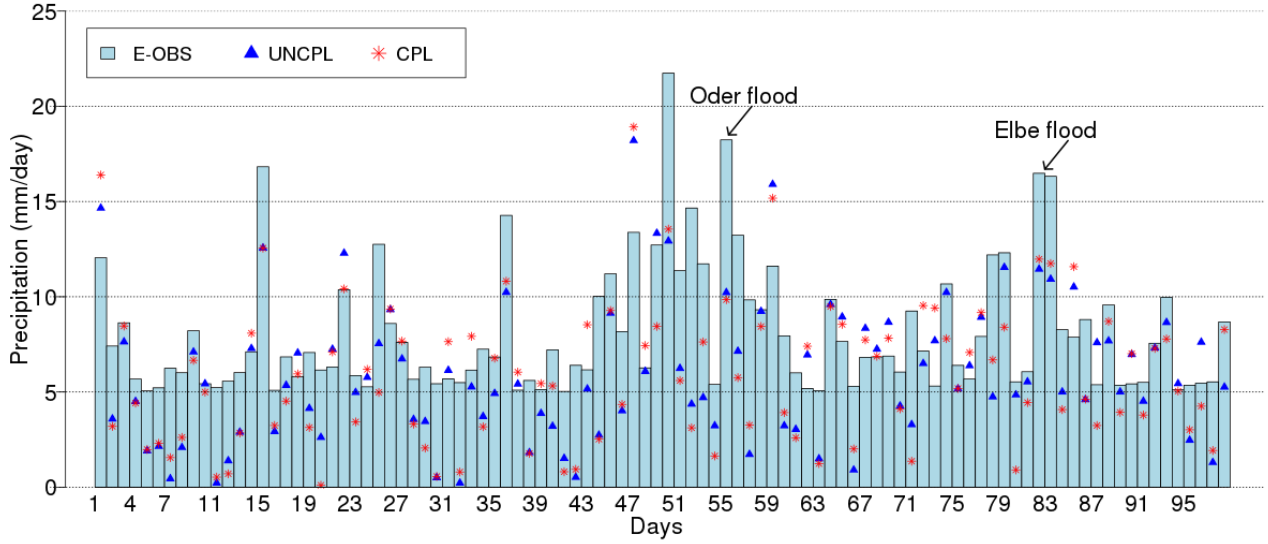

(e) UNCPL_HZG and CPL_HZG (v5.0, res. 0.22º)

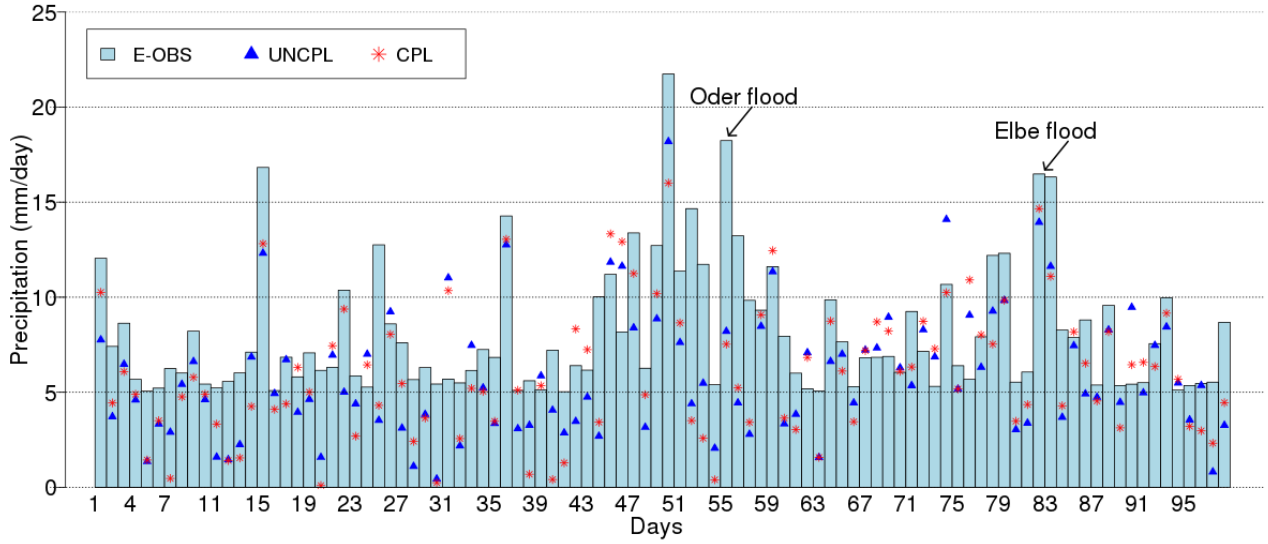

(f) Ensemble mean of all UNCPL & CPL

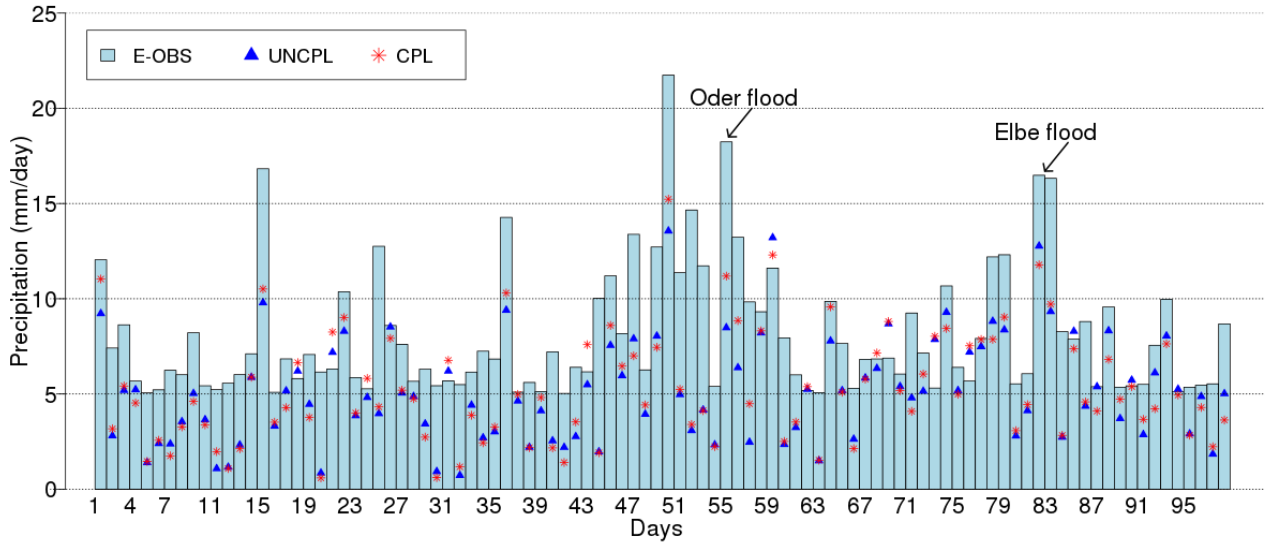

Fig.9 Daily precipitation (mm/day) of the E-OBS data (light-blue bars), uncoupled (blue triangles) and coupled (red asterisks) simulations averaged for Central Europe for 98 very wet days of the Northerly Circulation Type in JJA 1986-2009. (a) UNCPL_HZG and CPL_HZG v4.8; (b) Ensemble of UNCPL_HZG and CPL_HZG v4.8; (c) UNCPL_SMHI and CPL_SMHI; (d) UNCPL_HZG and CPL_HZG v5.0 on 0.44º grid; (e) UNCPL_HZG and CPL_HZG v5.0 on 0.22º grid; (f) Ensemble mean of all UNCPL and CPL experiments.

(a) Ensemble of UNCPL & CPL, including SMHI's simulations

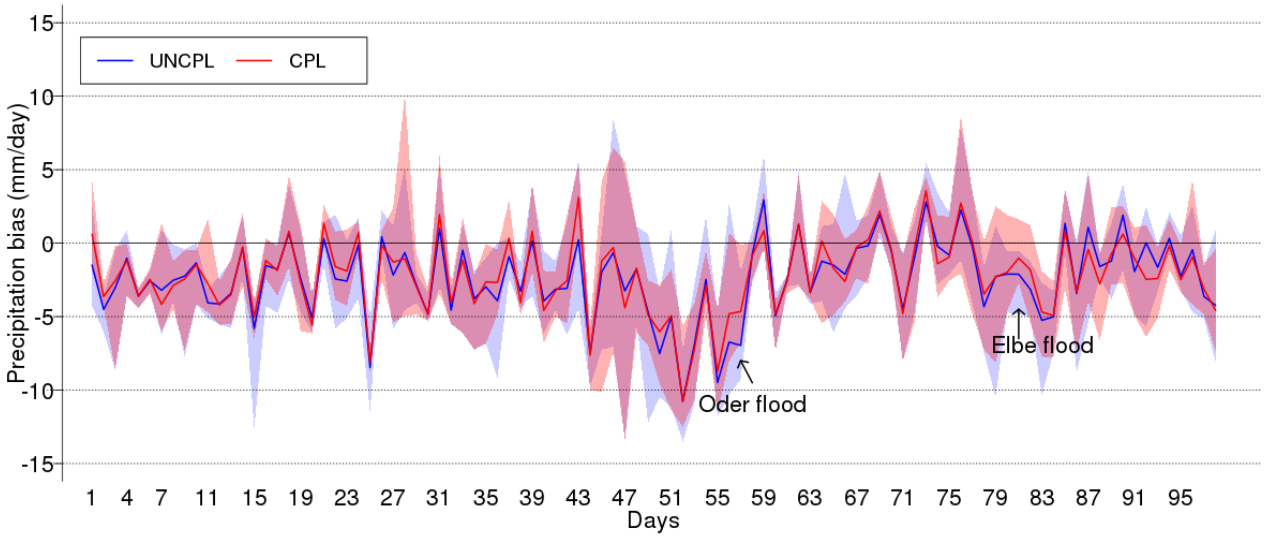

(b) Ensemble of UNCPL & CPL, excluding SMHI's simulations

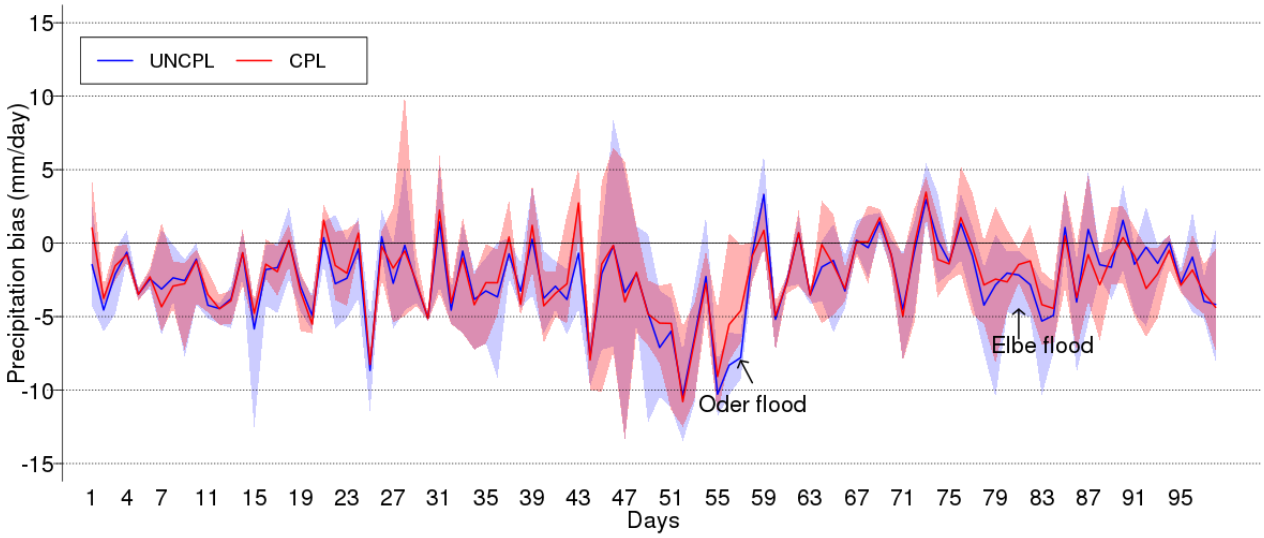

Fig.10 Daily precipitation bias (mm/day) of the ensemble of all uncoupled CCLMs (blue) and coupled CCLMs (red) experiments against the E-OBS data averaged for Central Europe for 98 very wet days of the Northerly Circulation Type in JJA 1986-2009. The shaded areas show ranges between minimum and maximum biases of the ensemble. The solid lines display the mean bias of the ensemble. (a) Including the SMHI's simulations; (b) Excluding the SMHI's simulations.

Appendix A: Differences in the (a) MSLP (Pa), (b) T_2M (K), (c) T_2M-T_S (K; atm-ocn), (d) moisture convergence (mm/day), (e) sensible heat flux (W/m2) and (f) latent heat flux (W/m2) between the CPL_HZG and UNCPL_HZG averaged for very wet days in JJA from 1986–2009 for the Northerly Circulation Type.

a)

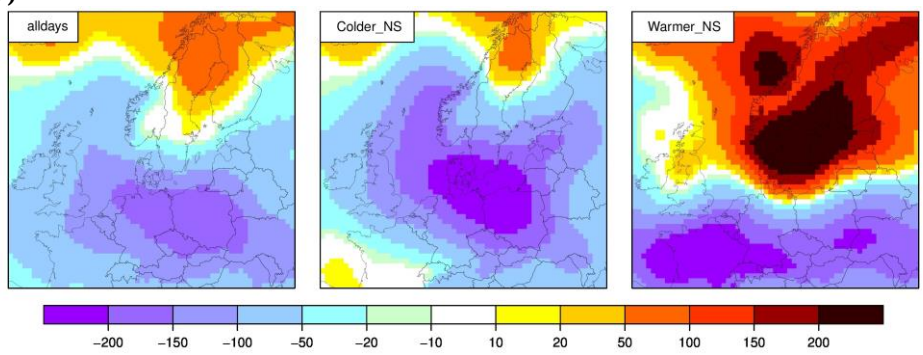

Mean sea level pressure (Pa)

b)

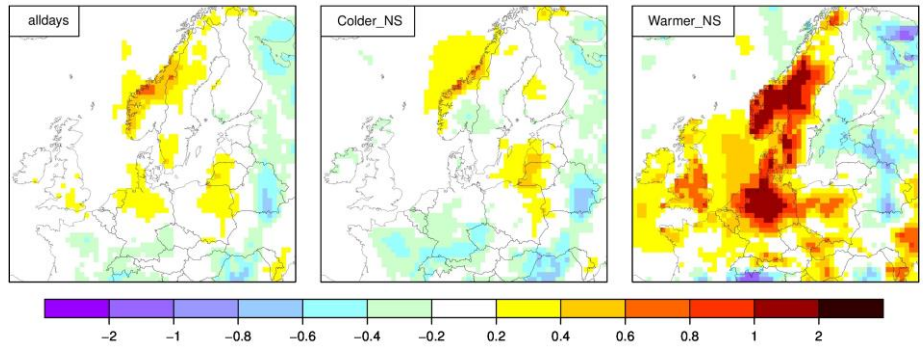

Air Temperature at 2m height (K)

c)

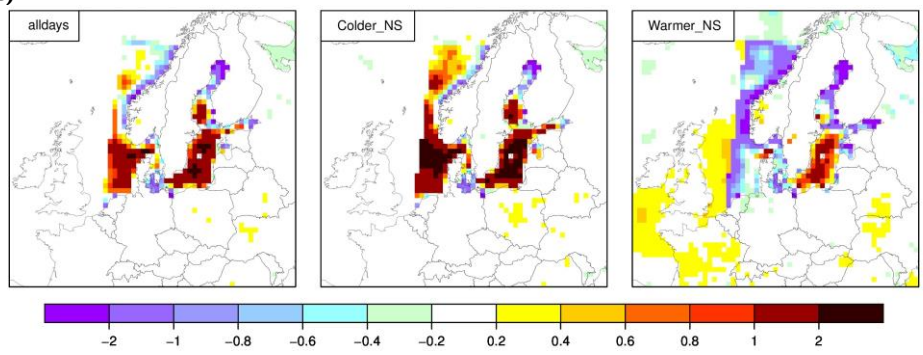

T_2M-T_S (K)

d)

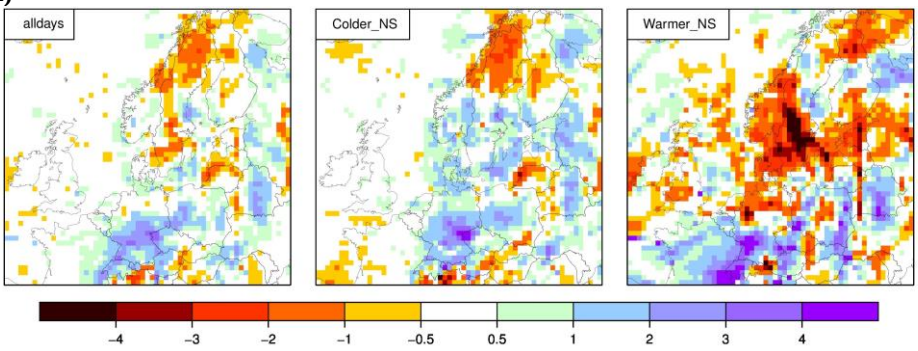

Moisture convergence (mm/day)

e)

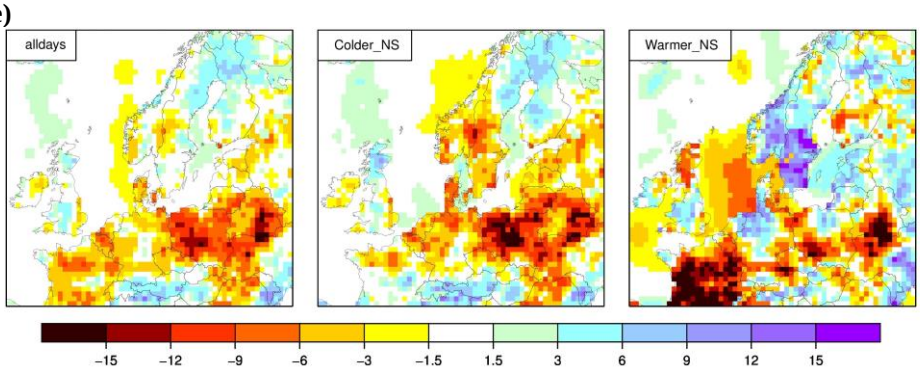

Sensible heat flux (W/m2)

f)

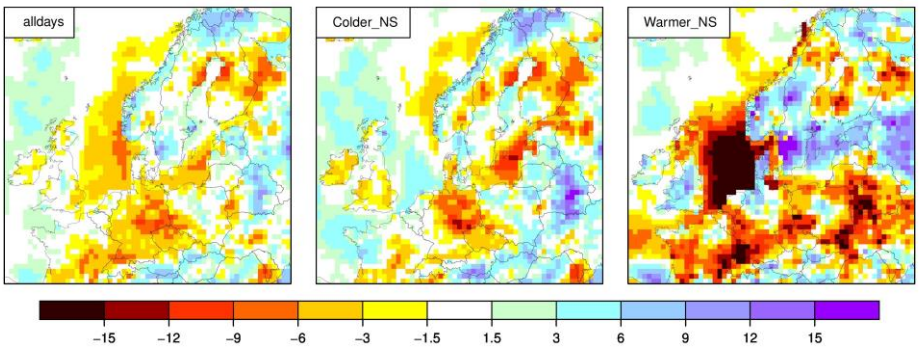

Latent heat flux (W/m2)